Ontogenetic and Regional Morphologic Variations in the Turkey Ulna Diaphysis: Implications for Functional Adaptation of Cortical Bone

JOHN G. SKEDROS,[1]* KENNETH J. HUNT,[1] PAUL E. HUGHES,[1] AND HOWARD WINET[2]

[1]Bone and Joint Research Laboratory, Department of Veterans Affairs Medical Center, Salt Lake City, Utah

[2]Bone Chamber Laboratory, J. Vernon Luck, M.D. Orthopaedic Research Center, Orthopaedic Hospital/UCLA, Los Angeles, California

ABSTRACT

This study examines relationships between bone morphology and mechanically mediated strain/fluid-flow patterns in an avian species. Using mid-diaphyseal transverse sections of domestic turkey ulnae (from 11 subadults and 11 adults), we quantified developmental changes in predominant collagen fiber orientation (CFO), mineral content (%ash), and microstructure in cortical octants or quadrants (i.e., %ash). Geometric parameters were examined using whole mid-diaphyseal cross-sections. The ulna undergoes habitual bending and torsion, and demonstrates nonuniform matrix fluid-flow patterns, and high circumferential strain gradients along the neutral axis (cranial-caudal) region at mid-diaphysis. The current results showed significant porosity differences: 1) greater osteocyte lacuna densities (N.Lac/Ar) (i.e., "non-vascular porosity") in the caudal and cranial cortices in both groups, 2) greater N.Lac/Ar in the pericortex vs. endocortex in mature bones, and 3) greater nonlacunar porosity (i.e., "vascular porosity") in the endocortex vs. pericortex in mature bones. Vascular and nonvascular porosities were not correlated. There were no secondary osteons in subadults. In adults, the highest secondary osteon population densities and lowest %ash occurred in the ventral-caudal, caudal, and cranial cortices, where shear strains, circumferential strain gradients, and fluid displacements are highest. Changes in thickness of the caudal cortex explained the largest proportion of the age-related increase in cranial-caudal breadth; the thickness of other cortices (dorsal, ventral, and cranial) exhibited smaller changes. Only subadult bones exhibited CFO patterns corresponding to habitual tension (ventral) and compression (dorsal). These CFO variations may be adaptations for differential mechanical requirements in "strain-mode-specific" loading. The more uniform oblique-to-transverse CFO patterns in adult bones may represent adaptations for shear strains produced by torsional loading, which is presumably more prevalent in adults. The micro- and ultrastructural heterogeneities may influence strain and fluid-flow dynamics, which are considered proximate signals in bone adaptation. Anat Rec Part A 273A:609–629, 2003. © 2003 Wiley-Liss, Inc.

Key words: bone adaptation; turkey ulna; collagen fiber orientation; osteocyte lacunae; osteons

A growing body of experimental data suggests that mechanical signals determine regional variations in the material organization of cortical bone (see Appendix A for definitions). The material organization of bone may, in turn, influence local mechanical behaviors. Within diaphyses of appendicular bones, such biomechanical adaptation can be manifested as regional variations in mineral content (%ash), microstructure (e.g., secondary osteon population density and porosity), and/or matrix ultrastructure (e.g., predominant collagen fiber orientation (CFO)). The adaptive effect appears to be most consistently expressed as variations in predominant CFO between regions habitually loaded in a prevalent strain mode (e.g., tension, compression, or shear) (Doden, 1987; Riggs et al., 1993a; Mason et al., 1995; Skedros et al.,

*Correspondence to: John G. Skedros, M.D., Bone and Joint Research Laboratory, Department of Veterans Affairs Medical Center, 500 Foothill Blvd. (151F/660), Salt Lake City, UT 84148. E-mail: jskedros@utahboneandjoint.com

Received 28 January 2003; Accepted 12 March 2003

DOI 10.1002/ar.a.10073

1996a, 1999; Martin et al., 1996a,b; Skedros and Kuo, 1999; Boskey et al., 1999; Puustjarvi et al., 1999; Takano et al., 1999; Skedros, 1994, 2001). It has been suggested that the consistent relationship between CFO and specific characteristics of a bone's strain history touches upon fundamental issues in skeletal biology, including growth, maintenance, homeostasis, and adaptation (Skedros, 2001; Skedros et al., 1996a, 2002a). This reasoning stems from in vivo strain gauge measurements on limb bones of various mammalian and avian species, which show that these bones typically demonstrate directionally constrained, habitual bending (Fritton and Rubin, 2001). This produces a spatially consistent tension/compression/shear strain distribution during peak loading of controlled physiologic activities, regardless of the animal's stage of development (Lanyon and Baggott, 1976; Lanyon et al., 1979; Biewener et al., 1986; Keller and Spengler, 1989; Indrekvan et al., 1991; Biewener and Bertram, 1993a; Biewener, 1993).[1]

It has been proposed that structural variations within appendicular long-bone diaphyses are most strongly selected to enhance "loading predictability" during typical use (Rubin, 1984; Lanyon, 1987; Bertram and Biewener, 1988; Swartz, 1993; Les, 1995; Skedros et al., 1996a). In the appendicular skeleton, loading predictability appears to be a major goal of a bone's adapted structural morphology. A predictable, controlled strain environment is readily achieved and accommodated by modeling processes, which produce variations in structural characteristics (including cortical thickness and cross-sectional shape), which in turn affect whole-bone stiffness and strength (Bertram and Biewener, 1988; Les, 1995; Skedros et al., 1996a). In contrast, regional remodeling activities produce material heterogeneities that result in important influences on local material properties. Consequently, structural as well as material adaptations may contribute to adaptation in limb bone diaphyses.

No structural or material characteristic has been shown to consistently correlate with habitual strain history or local strain patterns (Hunt and Skedros, 2001; Ohman and Lovejoy, 2001; Skedros, 2001). Furthermore, it is not clear to what degree regional variations in matrix porosities (e.g., central canals of secondary osteons, and osteocyte lacuna size and population density) or other regional microstructural and ultrastructural heterogeneities influence fluid-flow patterns produced by functional loading. These are important considerations, since strain- and fluid-flow-related stimuli influence bone development, adaptation, and maintenance (McLeod et al., 1998; Burger and Klein-Nulend, 1999; Srinivasan and Gross, 2000; You et al., 2001).

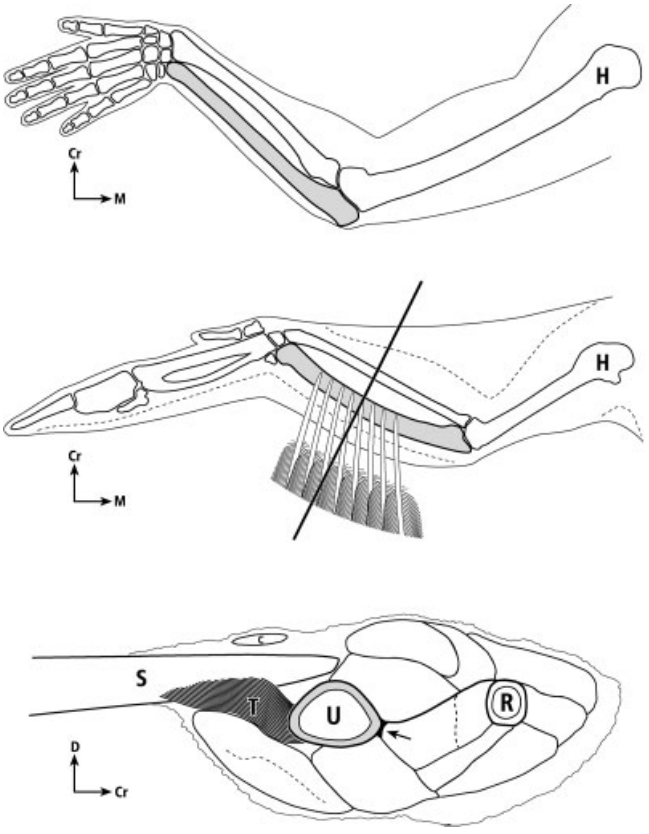

Fig. 1. Dorsal-to-ventral view of left upper extremity (human) and wing (avian). H, humerus; U, ulna (shaded); R, radius; Cr, cranial; D, dorsal; M, medial; T, "tether" of secondary feather (S) sheath (sheath = calamus wall; calamus = quill); C, secondary covert feather). The drawing at the bottom is a proximal-to-distal view of the left forelimb transversely sectioned at mid-diaphysis. A secondary feather is shown diagrammatically in profile; the remainder of the drawing represents the actual cross-section. There are 18 secondary feathers in domestic turkeys, and all of these "attach" along the ulna (Lucas and Stettenheim, 1972). (The upper two figures are modified from Figures 18-4 and 18-8 in the Guild Handbook of Scientific Illustrations (Hodges, 1989) with permission from the publisher and artist, Nancy Halliday.)

The mid-diaphyseal turkey ulna (Fig. 1) has become an important model for evaluating the mechanisms and manifestations of bone adaptation. It has been studied in terms of correlating bone remodeling and modeling with various types of mechanical loading and related fluid-flow dynamics (Rubin and Lanyon, 1985; Rubin and McLeod, 1996; Rubin et al., 1989, 1992, 1995, 1996; Adams et al., 1997; Fritton et al., 2000; Srinivasan and Gross, 2000; Qin et al., 1998). However, to our knowledge, no studies have attempted to describe both the structural and material organization of this bone during normal development. A primary goal of the present study was to examine bone morphology in the developing turkey ulna. We examine age-related structural variations that may also represent developmental functional adaptations, including cortical thickness and area, diaphyseal girth, longitudinal curvature, major axes of cross-sectional moments of inertia, and

[1]Mechanical strain is the change in length of a loaded structure as a percentage of its initial (unloaded) length. This unitless ratio is a measure of material or tissue deformation. In vivo strain data from a variety of animals suggest that physiologically normal strains are generally between 200 and 3,000 microstrain (i.e., 0.02–0.30% change in length) in compression (Rubin and Lanyon, 1985; Biewener et al., 1983a, b, 1986). The upper limit may be only 1,500 microstrain in tension (Fritton and Rubin, 2001). For an isotropic material loaded axially, stress and strain are related by Hooke's law, which says that they are proportional to one another. Available data suggest that strain is the mechanical parameter most directly involved in mediating bone adaptations (Rubin and Lanyon, 1984b; Lanyon, 1987).

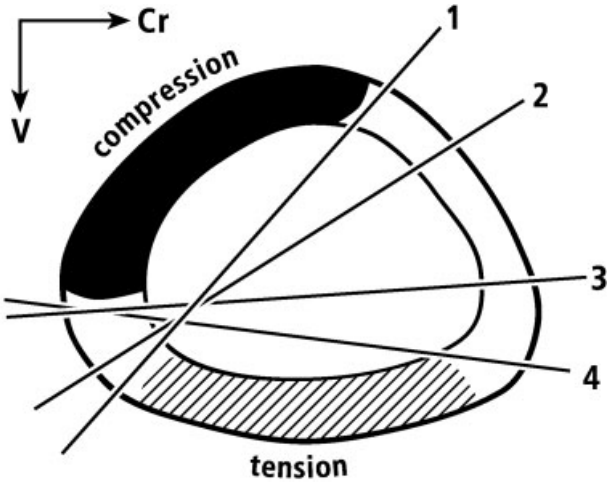

Fig. 2. Changes in the neutral axis at different times during the normal wing-flapping cycle (labeled lines 1–4). Adapted from Rubin and Lanyon (1985) with permission.

polar moments of inertia. Additionally, we describe material variations in the turkey ulna, including CFO, secondary osteon population density, secondary osteon cross-sectional area, and osteocyte lacuna size and population density. These results are discussed in the context of the habitual strain distribution and fluid-flow dynamics of this bone (Fig. 2).

MATERIALS AND METHODS

Specimen Preparation and Mineral Content Analysis

One ulna was randomly selected from each of 11 skeletally immature (subadult, 4–6 months old) and 11 skeletally mature (adult, 2 years old) male domestic ("broad-breasted white") turkeys. From each bone, two transversely cut 5.0-mm segments were obtained, one proximal to, and the other distal to the mid-diaphysis cut. Mid-diaphysis was defined as the midpoint between the center portions of the articular surface of each end of the bone. The segments were dissected free of soft tissue (including marrow), and the proximal segment was embedded in polymethyl methacrylate (PMMA) in an undecalcified state and prepared for ultramilling, as described below. Dry and ash weights were obtained for cranial, caudal, dorsal, and ventral cortical fragments of each distal specimen using previously described methods (Skedros et al., 1993a). Mineral content (%ash) was calculated by dividing the weight of the ashed bone (W_{AB}) by the weight of the dried, defatted bone (W_{DB}) prior to ashing, and multiplying this quotient by 100 [$(W_{AB}/W_{DB}) \cdot 100$].

Definition of Individual Locations (Octants), and "Tension" and "Compression" Regions

Micro- and ultrastructural analyses were conducted in the following cortical octants: dorsal (D), dorsal-cranial (D-Cr), cranial (Cr), ventral-cranial (V-Cr), ventral (V), ventral-caudal (V-Cd), caudal (Cd), and dorsal-caudal (D-Cd) (Fig. 3). Based on in vivo strain gauge data (Rubin and Lanyon, 1985) the D-Cd, D, and D-Cr cortices generally receive compression strains, and the V-Cd, V, and V-Cr cortices generally receive tension strains (Fig. 2). Cortices along the habitual neutral axis (Cr and Cd) generally receive shear strains. While shear strains exist throughout the bone cross section, they are the prevalent strain mode along the neutral axis. The micro- and ultrastructural characteristics of each octant were examined independently. For example, the dorsal and ventral cortices were analyzed for evidence of variations that may be adaptations to compression and tension, respectively.

Circularly Polarized Light Analysis

Predominant CFO was determined using 100 ± 5 μm ultramilled embedded sections viewed under circularly polarized light, according to published methods (Skedros et al., 1996a). Regional differences in CFO were inferred from corresponding differences in the intensity of transmitted light: darker gray levels (lower numerical values) represent relatively more longitudinal collagen, and brighter gray levels (higher numerical values) represent relatively more oblique-to-transverse collagen.

Mean gray-level values were quantified in 50× images (512 × 480 pixels; approximately 2.3 mm^2/image) in each octant of each immature and mature bone. In each location, the region analyzed was adjusted so that only the bone from the central 80% of the cortex was quantified. For example, care was taken to avoid the variably present, highly birefringent circumferential lamellar bone in the mature age group. The dorsal, ventral, cranial, and caudal locations of these sections were immediately proximal to the corresponding locations from which the ashed samples had been taken. The methods used to quantify regional CFO differences in cortical bone as differences in gray levels (Skedros et al., 1996a) have produced relative differences that are similar to the "longitudinal structure index" described by Martin and coworkers (Martin and Ishida, 1989; Martin et al., 1996a, b) and recently used by Takano et al. (1999) and Kalmey and Lovejoy (2002).

Microstructure

In addition to CFO, several other characteristics considered candidates for adaptive strain- and/or fluid-flow-related material heterogeneity were quantified (see Appendix B for abbreviations). The ultramilled specimens used in the CFO analysis were prepared for backscattered electron (BSE) imaging using published methods (Skedros et al., 1996a). Two 200× BSE images were obtained in each octant in immature specimens, and four 200× images (two endocortical and two pericortical) were obtained in each octant in mature specimens (Fig. 3). The following parameters were quantified for each image: 1) secondary osteon population density (N.On/Ar; no./mm^2); 2) fractional area of secondary bone (On.B/Ar; expressed as a percentage), 3) mean secondary osteon area (On.Ar; mm^2); 4) fractional area of porous spaces (Po/Ar, expressed as a percentage), excluding osteocyte lacunae and artifactual cracks; 5) population density of new remodeling events (NREs: resorption spaces plus newly forming osteons; no./mm^2); 6) osteocyte lacuna population density (N.Lac/Ar; no./mm^2); and 7) mean osteocyte lacunae area (Lac.Ar, μm^2).

In each image, N.On/Ar, On.B/Ar, Po/Ar, N.Lac/Ar, and Lac.Ar were quantified using algorithms of the public domain NIH image (v1.61) software (http://rsb.info.nih.gov/nih-image/). Osteocyte lacunae population density is meant to estimate the concentration of osteocytes, al-

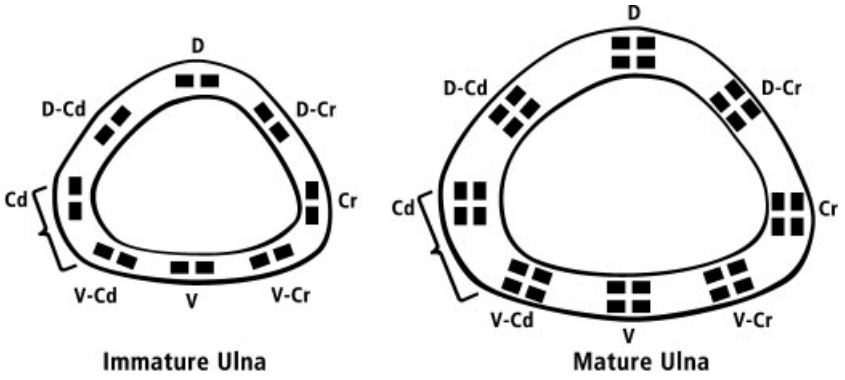

Fig. 3. Representative mid-diaphyseal transverse cross sections of an immature turkey ulna (left) and mature turkey ulna (right). Brackets indicate regions of insertion of the fibrous "tether" of the secondary feather sheaths. Dark rectangles indicate the locations where microscopic analyses were conducted. D, dorsal; D-Cr, dorsal-cranial; Cr, cranial; V-Cr, ventral-cranial; V, ventral; V-Cd, ventral-caudal; Cd, caudal; D-Cd, dorsal-caudal.

though no differentiation could be made between living and dead osteocytes. Average osteocyte lacuna area was based on the mean cross-sectional area of all lacunae in each image. The NIH image program was sufficiently sensitive to detect area differences of $<1\ \mu^2$.

Cracks (typically <2.0% of any image area) produced during tissue processing were eliminated from each image prior to quantifying porosity and On.B/Ar. Secondary osteons and secondary osteon fragments were traced in the NIH image program and manually counted. A secondary osteon was identified using previously described methods (Skedros et al., 1997). The On.B/Ar of each image and the cross-sectional area (mm^2) of each complete secondary osteon were calculated from these tracings using algorithms written for the program.

Mean areas of lacunae and complete osteons were made using an algorithm written for the NIH image program.

Histologic description. Using circularly polarized images, histology was categorized in accordance with the nomenclature used by Stover et al. (1992), de Margerie (2002), and de Ricqlès et al. (1991). Based on qualitative observations, primary bone was further distinguished into two general types (de Margerie, 2002): 1) laminar bone with predominantly circular primary osteons, and 2) laminar bone with predominantly oblique, radial, and longitudinal primary osteons.

New remodeling events (NREs). NREs include the sum of resorption spaces and newly forming secondary osteons. Two criteria were used to identify a newly forming secondary osteon: 1) the presence of relatively recently mineralized bone (gray levels that are relatively darker than surrounding bone in the BSE images), and 2) incomplete radial closure (i.e., incomplete centripetal deposition) of the recently mineralized bone. To determine whether the second criterion was satisfied, two mutually orthogonal lines (in cranial–caudal and dorsal–ventral directions) were drawn on each apparent newly forming osteon. Incomplete radial closure was defined as mineralized bone extending less than one-half of the osteon radius along two or more of the four possible radial locations (i.e., cranial, caudal, dorsal, or ventral).

Cortical Thickness, Bone Length, and Cross-Sectional Geometry

Cortical thickness and bone length. The following measurements were made to the nearest 0.01 mm using a digital vernier caliper (Mitutoyo™, Kanagawa, Japan): 1) bone "length" (the linear distance between the center of the proximal and distal articular surfaces), 2) overall subperiosteal dorsal–ventral "width" and cranial–caudal "breadth," and 3) cortical thickness at the dorsal, ventral, cranial, and caudal cortices.

Geometry. To quantify various cross-sectional geometric parameters and properties, endosteal and periosteal perimeters of the thin sections used for circularly polarized light analyses were traced with a digitizing pen (model 12 × 12; Kurta Corp., Phoenix, AZ) interfaced to a microcomputer. An adapted version of the computer program SLICE (Nagurka and Hayes, 1980) was then used to determine the following from each tracing: 1) total subperiosteal area (TA); 2) cortical area (CA); 3) major axis (Imax) and orthogonal minor axis (Imin) of the second moment of area (inertia, I); 4) Φ angle, which represents the angle subtended by Imax and the anatomic cranial-caudal axis in the dorsal direction; and 5) polar moment of inertia (J = Imax + Imin). The CA:TA ratio and the polar moment of inertia (J = sum of moments of inertia along the major axis [Imax] and orthogonal minor axis [Imin]) were calculated for each section. According to engineering principles, 1) the total bone cross-sectional area (excluding marrow) in beam-like structures provides an estimate of axial compressive or tensile strength, 2) the CA:TA ratio provides an estimate of robusticity, 3) J is indicative of a beam's torsional and bending rigidity, 4) the Imax:Imin ratio provides information about the cross-sectional shape and distribution of the material, and 5) the orientation of Imax (Φ angle) denotes the direction of greatest bending resistance (rigidity) at the cross-section location (Ruff, 1981, 1989; Ruff and Hayes, 1983; Swartz, 1993). The Imax:Imin ratio indicates the degree to which the bone cross-section deviates from the purely circular. If this ratio differs substantially from one, then the whole bone strength index (see below) will not accurately estimate bending strength if the loads in the directions of Imax and

Imin are not directly proportional to I in these two directions. This was not deemed applicable to the values reported in the present study.

Section modulus (Z) and bone strength index (BSI) were calculated for each bone (van der Muelen et al., 1996; Alexander, 1998):

$$Z = J/D$$

where J is the polar moment of inertia and D is the mean diameter of the cross section (Heinrich et al., 1999). Using these data and bone length (L), BSI was calculated:

$$BSI = J/DL = Z/L.$$

The BSI is proportional to the ultimate stress required to fracture a bone when held by its ends while a transverse force is applied at mid-diaphysis (van der Muelen et al., 1996).

Considerations of Regional Modeling Activities (Cortical Drift)

Preferential direction(s) in cortical modeling drifts were estimated by examining changes in: 1) cross-sectional geometry and cortical thickness (as described above), 2) interosseous distance (i.e., between the radius and ulna), and 3) diaphyseal curvature.

Interosseous distance. The average distance between the cranial cortex of the ulna and the caudal cortex of the radius was measured on mature and immature turkey limbs at mid-diaphysis. Measurements were made on each specimen with the wing in extension so that the proximal radial and ulna articular surfaces were congruent.

Diaphyseal longitudinal curvature. Gross observations were made to determine whether the ulnar diaphyseal curvature changed between the two age groups. Ulnae from each group were placed on an osteometric table. Each bone was viewed in a cranial–caudal direction, with the bone beneath a taught strand of monofilament line that intersected the center of the distal and proximal articular surfaces. We noted whether or not the line intersected the bone at mid-diaphysis.

Observations of Gross Dissection

Several additional wings were cut and dissected in order to provide illustrative material to clarify: 1) the muscular cross-sectional anatomy at the mid-diaphyseal ulna and radius, and 2) the functional morphology of secondary feather insertion. These are important considerations, since both may have important local influences on diaphyseal loading.

Statistical Analysis

Pairwise comparisons between cortical regions of each species were assessed for statistical significance using a one-way analysis of variance (ANOVA) with Fisher's least significant post-hoc test (Stat View version 5.0; SAS Institute Inc., Cary, NC) (Sokal and Rohlf, 1995). Testing for assumptions of normally distributed data (NCSS 6.0, Number Cruncher Statistical Systems, Dr. Jerry Hintze, Kaysville, UT) revealed that 10% of the geometry data subsets and 27% of the microstructure data subsets were not normally distributed. None of the geometry data subsets and only 13% of microstructure data subsets showed distributions that were J-shaped or severely skewed (defined as skewness values of >1.0 or < -1.0). According to Kachigan (1986), parametric tests are more powerful in this situation than the alternative nonparametric test, provided that a P-value of <0.01 is used for the non-normally distributed data sets. Thus, we report results of parametric testing using a one-way analysis of variance (ANOVA) and Fisher's LSD post-hoc test using a P-value of <0.05 for statistical significance. For non-normally distributed data sets, a P-value of <0.01 was considered statistically significant. Means $\pm$ standard deviations (S.D.s) are reported.

Two-way ANOVAs were conducted on the mature bones using data from octant locations as well as from pericortical vs. endocortical regions. Pearson correlation coefficients for various comparisons were determined within each group. The magnitudes of the resulting correlation coefficients (r) were interpreted according to the classification of Hinkle et al. (1979). In this scheme, coefficients in the ranges of 0.9–0.99, 0.7–0.89, 0.5–0.69, 0.3–0.49, and 0.0–0.29 are interpreted as representing very high, high, moderate, low, and little if any correlation, respectively.

RESULTS

Regional and Age-Related Histology

Compared to the adult bones, the subadult specimens exhibited laminar bone (plexiform and simple primary osteonal bone, sensu Stover et al. (1992)) with a prevalent longitudinal, radial, and oblique primary osteons (de Margerie, 2002) (Fig. 4B). Radial and oblique primary osteons predominated in the cranial and caudal regions. Periosteal and endosteal circular laminar bone, resembling circumferential lamellae, and secondary osteons in adults (see below) were not seen in subadult bones.

Representative microscopic images from adult bones appear in Figures 4A and 5. Adult specimens exhibited mature plexiform bone (laminar bone with circular primary osteons, sensu de Margerie (2002)) with a greater prevalence of longitudinal, radial, and oblique primary osteons (de Margerie, 2002) in regions along the cranial-caudal axis (Fig. 4A). Circular primary osteonal bone, resembling circumferential lamellar bone, was prevalent along the periosteal and endosteal surfaces.

In adult bones, secondary osteons were concentrated along the cranial–caudal axis (described below) (Fig. 5). When viewed under polarized light, the majority of these secondary osteons (>80%) were of the lamellar type described by Marotti (1996, Table II). Parallel-fibered osteons were seen in the regions of insertion of the secondary feather sheath "tethers."

CFO: Analysis of Combined "Tension" and "Compression" Regions and Individual Octants

Combined regions. Both age groups showed relatively more oblique-to-transverse CFO in the "compression" region (D-Cd, D, D-Cr) than in the "tension" region (V-Cd, V, V-Cr), as demonstrated by higher mean gray levels in the "compression" regions ($P < 0.0001$) (Figs. 2 and 6). In contrast, there were no significant mean gray-

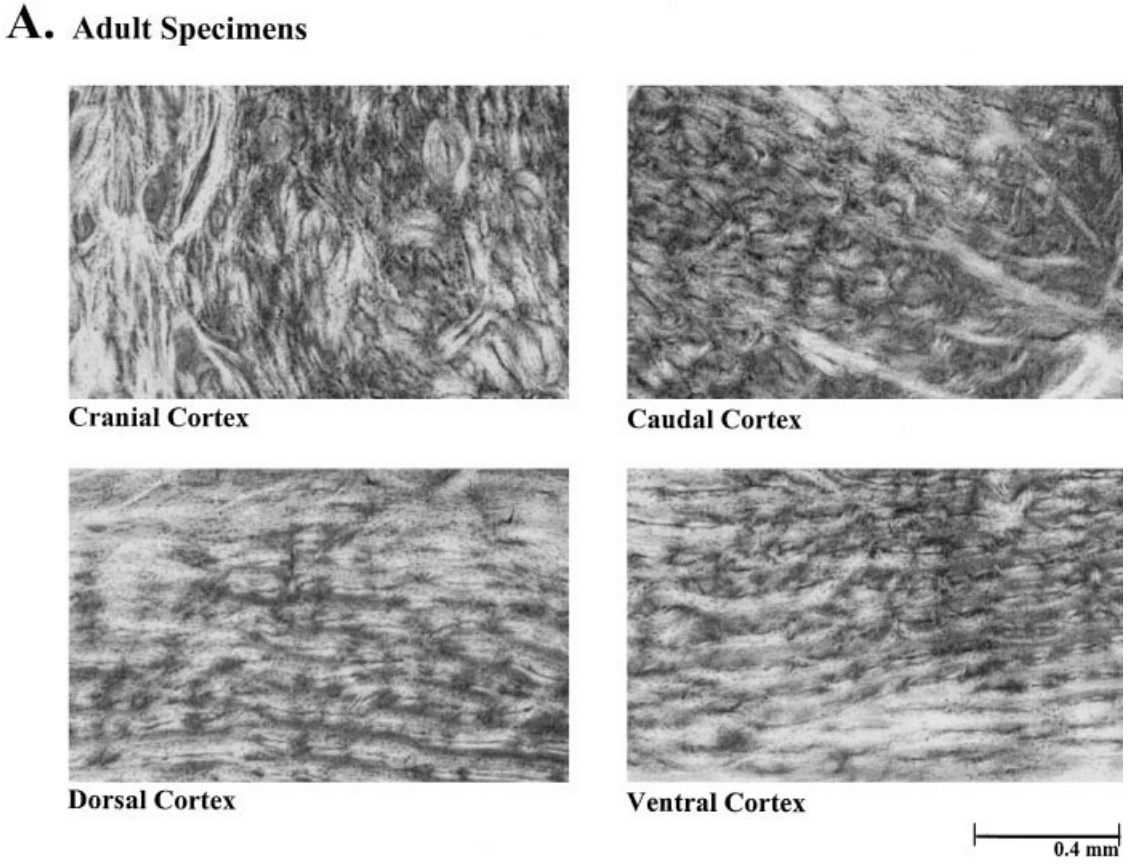

Fig. 4. Circularly polarized light images of adult (**A**) and subadult (**B**) bones. Images were taken at 50× magnification.

level differences between the cranial vs. caudal (neutral axis, "shear") regions in each age group (7% difference in mature bones, $P = 0.11$; 5% difference in immature bones, $P = 0.27$).

Octants. In contrast to the significant CFO differences shown between the combined "tension" and "compression" regions in both age groups, only the subadult bones showed such differences between individual cortical octants (Fig. 6). In other words, the dorsal and ventral cortices, which are predominant "compression" and "tension" locations, respectively, show a "strain-mode-specific" pattern only in the immature bones. In adult bones, a relatively more uniform CFO pattern occurred. Specifically, the ventral and ventral-caudal ("tension") cortices have collagen fibers with oblique-to-transverse orientation, similar to the "compression" locations.

Microstructure, Mineral Content, and Cortical Thickness

Immature bones (porosity, N.Lac/Ar, Lac.Ar, and mineral content). The NIH image program consistently produced results that were within 2.5% of the results obtained from a set of randomly selected, manually counted images (N.Lac/Ar) or point-counted (On.B/Ar & Po/Ar) images (Skedros et al., 1994b, 1997). No secondary osteons were found in immature specimens. Cranial and caudal cortices (i.e., the neutral axis regions) had the highest N.Lac/Ar and Lac.Ar (Figs. 7 and 8; $P < 0.0001$). Nonlacuna porosity, which consists mainly of primary vascular canals (and excludes microporosities such as canaliculi and microcanaliculi), was lowest in dorsal, dorsal-caudal, and caudal cortices ($P < 0.05$). Nonlacuna porosities in the other cortices were not significantly different ($P > 0.23$). The lowest mineral content (%ash) was found in the caudal cortex of immature bones (Cd = 67.9%, Cr = 68.7%, D = 69.4%, V = 68.6%) ($P < 0.05$ for caudal vs. each of the other regions except ventral, where $P = 0.08$). Although the %ash differences between cranial vs. dorsal and dorsal vs. ventral cortices were small, they were also statistically significant ($P = 0.045$ and $P = 0.015$, respectively).

Mature bones (porosity, N.Lac/Ar, Lac.Ar, mineral content, N.On/Ar, On.B/Ar, On.Ar, On.Shp, and NREs). In mature bones, significant regional microstructural differences occurred in the ventral-caudal, caudal, and cranial cortices (V-Cd approximates the "tension" region, while Cr and Cd are predominantly "neutral axis" regions) (Fig. 9). Compared to the averaged values of the other octant locations, the ventral-caudal cortex has an average of 700% higher N.On/Ar ($P < 0.001$) and 500% higher On.B/Ar ($P < 0.001$).

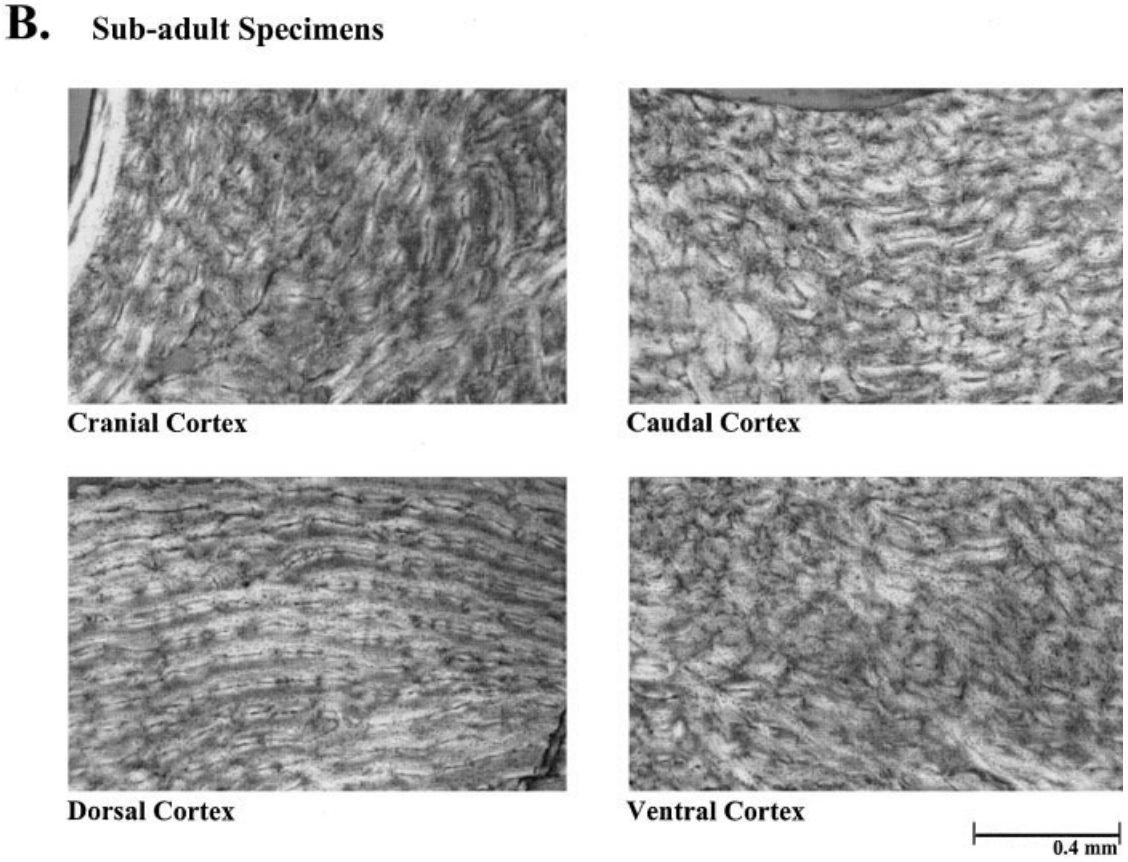

Figure 4. Continued.

The caudal cortex contained the greatest population of NREs compared to all other cortices ($P < 0.05$). The dorsal and ventral cortices contained the fewest, if any, NREs.

The caudal cortex also had lower %ash (Cd = 68.9%, Cr = 70.2%, D = 70.0%, V = 70.1%) ($P < 0.05$ for caudal vs. each of the other regions). In adult turkey ulnae, there were no significant %ash differences between the cranial, ventral, and dorsal cortices ($P > 0.6$).

Both the cranial and caudal cortices of mature bones demonstrated significantly greater N.Lac/Ar than all other cortices (Fig. 7; $P < 0.001$); however, the caudal cortex contained significantly more N.Lac/Ar compared to the cranial cortex ($P = 0.014$).

Differences in Lac.Ar were also present in mature bones. The ventral cortex had the highest average Lac.Ar, and was significantly higher compared to nearly all other cortices ($P < 0.0001$), except the caudal ($P = 0.93$) and cranial ($P = 0.42$) cortices (Fig. 8). There was no significant difference between the caudal and cranial cortices ($P = 0.37$).

The average area of osteons (On.Ar) in "compression" regions (D-Cd, D, D-Cr) tended to be smaller than in "tension" regions (V-Cd, V, V-Cr) ($P = 0.08$) and neutral axis or "shear" (Cr, Cd) regions ($P = 0.08$).

Pericortical vs. endocortical comparisons. Relative to pericortical regions, the endocortical region of mature bones had a greater mean lacuna area (21.8 μm^2 vs. 20.8 μm^2, $P < 0.0001$). The endocortical region also had greater nonlacunar ("vascular") porosity, but this was not statistically significant ($P = 0.16$). Differences in predominant CFO, N.Lac/Ar, and all other microstructural variables were not statistically significant between pericortical and endocortical regions.

Two-way ANOVAs in individual octants showed a higher average lacuna area (Lac.Ar) in the endocortical region compared to the pericortical region in each of the eight cortices; this was significant only in caudal, ventral-caudal, and ventral cortices ($P < 0.05$), and was a trend in dorsal, dorsal-cranial, and cranial cortices ($0.05 < P < 0.1$). N.Lac/Ar was generally higher in the pericortical region than the endocortical region, but this was only significant for the cranial cortex ($P < 0.05$). Average "vascular" porosity was greatest in endocortical regions of all but two cortices (D-Cd and D-Cr), but this difference was significant only in the dorsal cortex ($P < 0.05$).

Mean Data of Entire Cross Section

When data were averaged for the entire cross section, immature bones showed significantly greater nonlacunar porosity (4.5% ± 1.5% vs. 3.8% ± 2.6%; $P < 0.0001$) and higher N.Lac/Ar (1314.9 ± 307.5 vs. 1049.5 ± 184.8; $P < 0.0001$) than mature bones. The average area of osteocyte lacunae tended to be greater in immature bones (21.7μm^2 vs. 21.3μm^2, $P = 0.054$). Whole-bone CFO (i.e., mean of all regions for each bone) was more oblique-to-transverse in

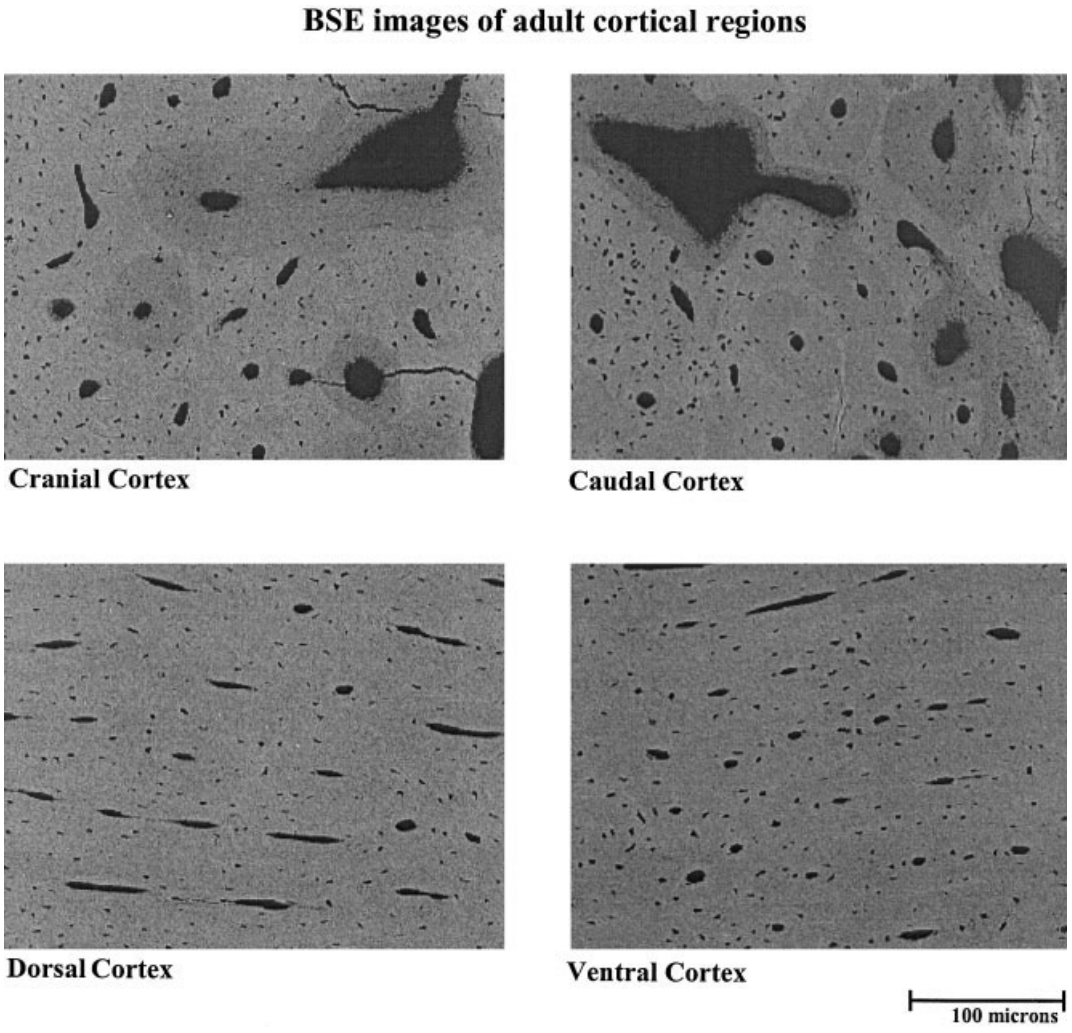

Fig. 5. Backscattered electron images of an adult turkey ulna. Images were taken at 200× magnification.

adult bones compared to subadults (147.5 ± 8.9 vs. 134.5 ± 10, respectively; $P < 0.01$). Whole bone %ash was greater in adults compared to subadults (69.8 ± 0.65 vs. 68.7 ± 0.52, respectively; $P < 0.01$).

Length, Cortical Thickness, Cortical Area, Imax, Imin, J, Φ angle, Z, and BSI

Length and cortical thickness. The average bone "lengths" were 12.0 ± 0.4 cm and 17.0 ± 1.1 cm in immature and mature bones, respectively. In immature bones, the cranial cortex was 20% thicker than the dorsal, ventral, and caudal cortices (mean difference: 0.33 mm, $P < 0.01$). In mature bones, the caudal cortex was 28% thicker than the dorsal, ventral, and cranial cortices (mean difference: 0.48 mm, $P < 0.001$). Comparisons of caudal thickness and cranial thickness as a percentage of cranial-caudal breadth showed that in mature bones, the caudal cortex accounts for a greater relative increase in total cranial-caudal breadth than the cranial cortex ($P < 0.001$). The ratio of the cranial-caudal breadth to dorsal-ventral width increases slightly with age (1.30 vs. 1.34, $P < 0.01$). Except for changes in the thickness of the caudal cortex, the thickness of the other cortices (D, V, Cr) remained relatively unchanged (Table 1).

Cortical area vs. total area. As expected, both cortical area and total cross-sectional area increased during the maturation interval examined. However, the ratio of cortical area to total area (CA:TA) did not change between age groups (0.54 vs. 0.52, $P = 0.15$; Table 1).

Imax, Imin, J, and Φ angle. The ratio of Imax:Imin increased with age (immature = 1.31 vs. mature = 1.47, $P < 0.05$). The Φ angle (the deviation of Imax from the cranial-caudal axis in the dorsal direction) decreased slightly with age, but this was not statistically significant (7.7° vs. 5.3°, $P = 0.19$; Table 1). Consequently, the increased cortical thickness along the cranial-caudal axis (the predominant neutral axis during functional loading) had a much greater influence on changes in the

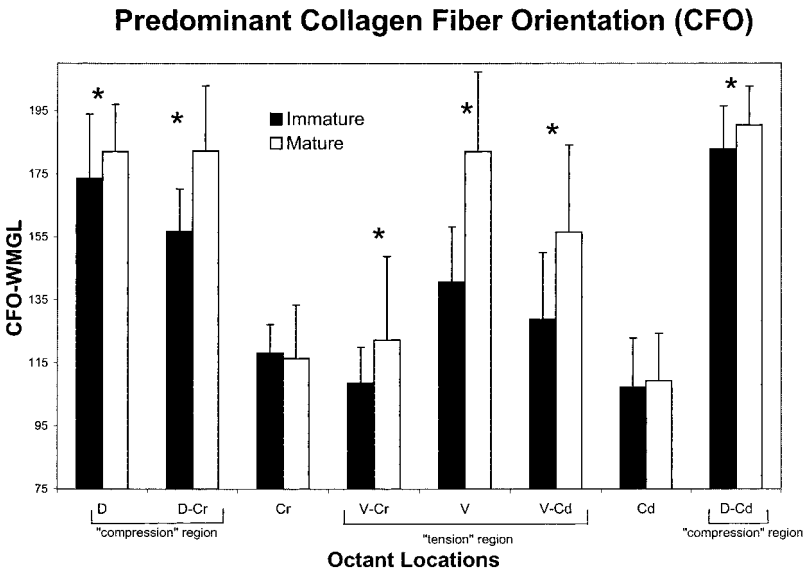

Fig. 6. Mature bones had more oblique-to-transverse collagen (higher WMGL) than immature bones in both the "tension" region (V-Cr, V, V-Cd, $P < 0.05$) and "compression" region (D-Cd, D, D-Cr, $P < 0.05$). There were no significant differences in the "neutral axis" (cranial-caudal) regions ($P > 0.5$). The compression region showed more oblique-to-transverse collagen when compared to the tension region in both age groups ($P < 0.001$). However, when individual octants were considered, only the immature bones showed tension (ventral) vs. compression (dorsal) differences. * = $P < 0.05$ for subadult to adult paired comparison.

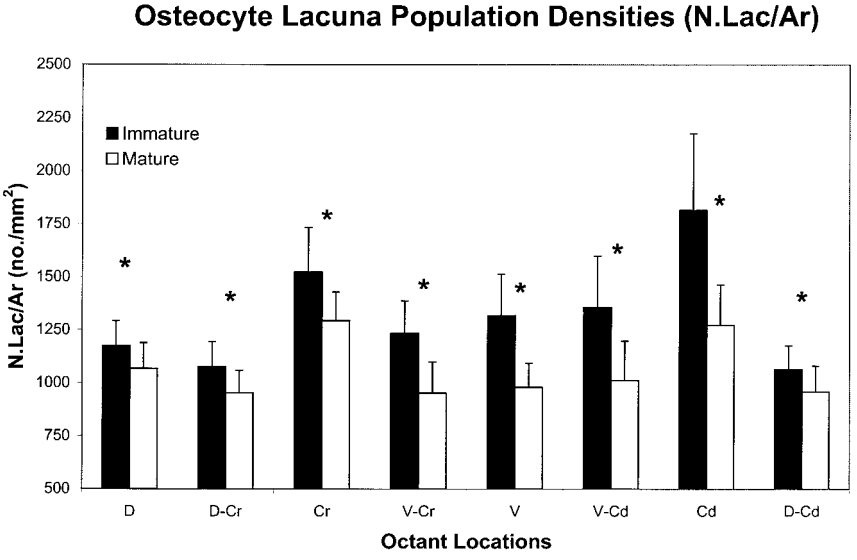

Fig. 7. In all cortical octants, immature bones have greater N.Lac/Ar than mature bones. N.Lac/Ar decreased by 30% in the caudal cortex with age, compared to an average age-related reduction of 10% over all seven other cortices. * = $P < 0.01$ for subadult to adult paired comparison.

cross-sectional moment of inertia (Imax) relative to the orthogonal (dorsal-ventral) axis.

BSIs. The BSI was significantly higher in adult bones compared to subadult bones (Table 1). This was more a function of section modulus (Z) than length. Individual correlations between BSI, whole-bone ash content, and whole-bone CFO are shown in Table 2. "Whole bone" refers to the mean value obtained from all regions (eight regions for CFO; four regions for ash) in each bone.

Regression Analyses

Octants. All correlations are reported in Tables 2 and 3. Regression analysis in the mature bones showed a low negative correlation between CFO and N.Lac/Ar ($r = -0.386$, $P < 0.01$) and a low positive correlation between N.Lac/Ar and Lac.Ar ($r = 0.355$, $P < 0.001$). In immature bones, there was also a moderate negative correlation between CFO and N.Lac/Ar ($r = -0.581$, $P < 0.0001$) and a high positive correlation between N.Lac/Ar and Lac.Ar

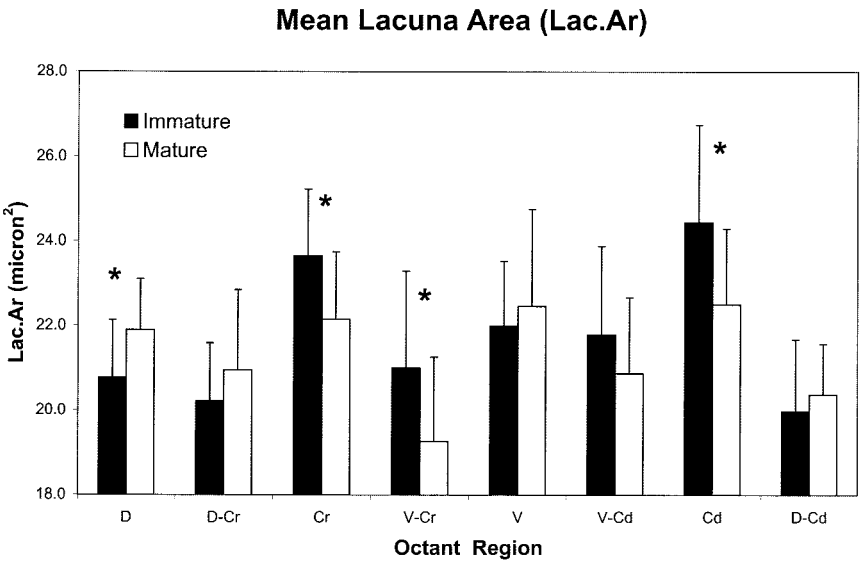

Fig. 8. Each of the cranial, ventral-cranial, and caudal cortices have lacunae with greater mean area in immature bones compared to mature bones ($P < 0.01$). The dorsal cortex of immature bones has a lower average lacuna area compared to that of mature bones. * = $P < 0.05$

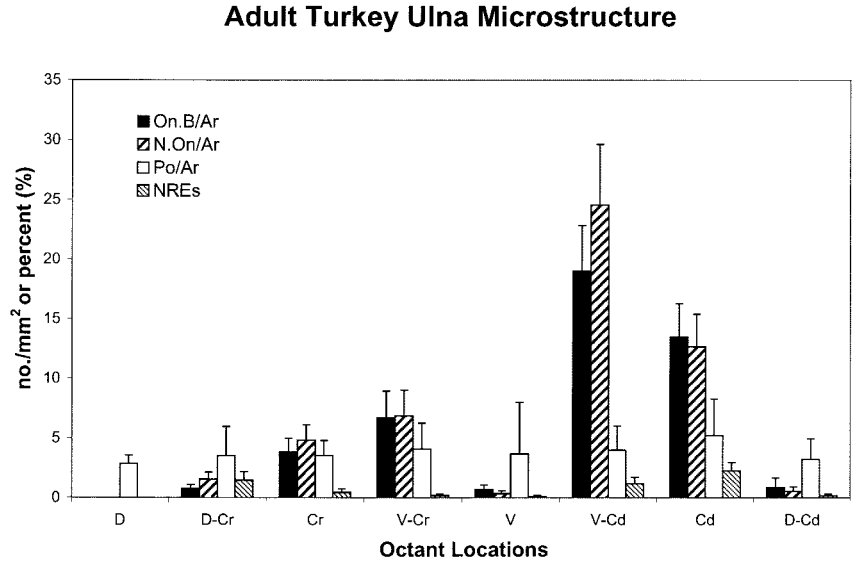

Fig. 9. In mature bones, compared to all other octant locations, the ventral-caudal (V-Cd) cortex has the highest On.B/Ar and the highest N.On/Ar ($P < 0.001$). The caudal (Cd) cortex has more N.On/Ar and higher On.B/Ar than all cortices, except for the V-Cd cortex, and the caudal cortex shows greater porosity than all other cortices ($P < 0.05$).

(r = 0.718, $P < 0.001$). There was a moderate positive correlation between CFO and Lac.Ar in immature bones (r = 0.417, $P < 0.001$).

Inferences of Cortical Drift: Interosseous Ulna-to-Radius Distance, Diaphyseal Curvature, and Cortical Thickness Variations

The distance between the radius and ulna (i.e., the interosseous distance; see Fig. 1) at mid-diaphysis was significantly different between immature (13.4 ± 1.1mm) and mature (17.0 ± 1.9mm) ($P < 0.001$) bones. Gross observations of diaphyseal curvature indicated that in all bones the periosteal surface of the ventral cortex was dorsal to the line intersecting the centers of the proximal and distal articular surfaces. Gross observations also suggested that both age groups had proportionally similar magnitudes of longitudinal curvature at mid-diaphysis.

Observations of Dissections

The cross-sectional muscular anatomy at mid-diaphysis is shown in Figure 10. The muscle bellies loosely adhere to the cortex with gossamer-like Sharpey's fibers. However, there are two exceptions where there are firm insertions to the cortex: 1) three muscles insert firmly along the cranial

TABLE 1. Cortical thickness and geometry of immature and mature bones (mean values S.D.)

Cortical thickness data (in mm)[a]

Age group	Wd	Br	D	V	Cr	Cd	Br/Wd	D/V	Cr/Cd	D/Wd	V/Wd	Cr/Br	Cd/Br
Mature	11.14 (0.43)	14.54 (0.65)	1.66 (0.17)	1.58 (0.24)	1.93 (0.23)	2.21 (0.28)	1.31 (0.03)	1.07 (0.11)	0.88 (0.12)	0.15 (0.02)	0.14 (0.03)	0.13 (0.02)	0.15 (0.02)
Immature	8.14 (0.20)	10.92 (0.47)	1.18 (0.21)	1.21 (0.22)	1.61 (0.18)	1.46 (0.14)	1.34 (0.04)	0.98 (0.18)	1.11 (0.11)	0.14 (0.03)	0.15 (0.03)	0.15 (0.02)	0.13 (0.01)
P value	**<0.001**	**<0.001**	**<0.001**	**<0.001**	**<0.001**	**<0.001**	**0.0034**	0.084	**<0.001**	0.450	0.470	**0.021**	**0.013**

Geometry data (areas in mm^2, moments in mm^4)[b]

Age group	CA	TA	CA/TA	Imax	Cd	Imin	Imax/Imin	ϕ	J	Z	BSI
Mature	65.91 (4.17)	127.44 (13.67)	0.52 (0.04)	1203.9 (217.9)		824.5 (158.3)	1.47 (0.14)	5.3 (1.0)	2028.4 (365.9)	160.4 (22.7)	11.3 (1.4)
Immature	38.26 (4.44)	70.06 (5.67)	0.55 (0.04)	357.7 (72.6)		273.5 (44.6)	1.31 (0.16)	7.7 (1.5)	631.2 (115.6)	66.2 (9.8)	5.55 (0.8)
P value	**<0.001**	**<0.001**	0.149	**<0.001**		**<0.001**	**0.018**	0.194	**<0.001**	**<0.001**	**<0.001**

[a]Wd, dorsal-ventral subperiosteal width; Br, cranial-caudal subperiosteal breadth; D, dorsal; V, ventral; Cr, cranial; Cd, caudal.
[b]CA, cortical area; TA, total area; Imax, major axis of second moment of inertia; Imin, orthogonal (to Imax) axis of second moment of inertia; J, polar moment of inertia; ϕ (phi), represents the angle subtended by Imax and the anatomic cranial-caudal axis, and the phi angle deviates toward the dorsal cortex; Z, section modulus; BSI, bone strength index.
P value represents the mature v.s. immature comparison. Bolded values are statistically significant ($P < 0.05$).

TABLE 2. All bones (*r* values)

	WB CFO	WB ASH	BSI
WB CFO	1.000		
WB ASH	0.488[a]	1.000	
BSI	0.564[b]	0.682[b]	1.000

[a]$P < 0.05$.
[b]$P < 0.01$.
WB, whole bone (i.e., mean of all regions for each bone); BSI, bone strength index.

cortex in a location that approximates the expected attachment of an interosseous membrane (see arrow in Fig. 10), and 2) a fibrous "tether" extends from each secondary feather sheath and firmly attaches to the caudal cortex (see "T" in Fig. 10). Unlike the loose muscle attachments, these firm attachments had to be released with a knife. The feather tip (calamus) and its vascular supply lie within a fascial septum dorsal to the dorsal ulnar cortex. During wing flapping (feather adduction/abduction) and other feather movement (e.g., flexion/extension during wing extension), it appears that the fibrous tether directly loads the caudal cortex. Unlike the continuous muscle coinsertion along the cranial aspect, these tethers (of which there are 18) form comparatively discrete insertions along the caudal aspect of the ulna.

DISCUSSION

A common approach to interpreting the mechanical relevance of variations in a bone's regional structural and material organization is to correlate them with a "habitual" loading history. During normal wing-flapping, the mid-diaphyseal turkey ulna experiences preferential bending in the dorsal-ventral direction; the dorsal cortex receives prevalent compression strains and the ventral cortex receives prevalent tension strains (Rubin and Lanyon, 1985). However, superimposed on this bending is a significant amount of torsion (producing significant shear stresses and strains), as evidenced by rotation of the neutral axis by nearly 70° during normal wing-flapping activities (Fig. 2). Even though the neutral axis shifts so dramatically, the dorsal and dorsal-caudal cortices still receive net compression, and the ventral cortex receives net tension during these activities (Rubin and Lanyon, 1985; Rubin and Lanyon, 1987; Fritton et al., 2000). The results of the present study are considered in the context of this loading history.

CFO and Histologic Observations

Regional "strain-mode-specific" CFO patterns have been reported in various limb bones, including diaphyseal regions of ovine, cervine, and equine calcanei, equine radii and third metacarpals, ovine radii, human proximal femoral diaphyses, and chimp femoral necks (Lanyon and Baggott, 1976; Lanyon et al., 1979; Portigliatti Barbos et al., 1983, 1984; Ascenzi et al., 1987; Carando et al., 1989, 1991; Riggs et al., 1993a, b; Mason et al., 1995; Martin et al., 1996a, b; Skedros and Kuo, 1999; Skedros, 2001; Skedros et al., 1994a, 1996a, 1999, 2002a; Kalmey and Lovejoy, 2002). This "strain-mode-specificity" is manifested as predominantly longitudinal collagen in cortical locations receiving predominant tension, and predominantly oblique-to-transverse collagen in cortical locations receiving predominant compression.

TABLE 3A. Correlations: Adult bones (*r* values)

	N.On/Ar	On.B/Ar	NREs	On.Ar	Po/Ar	N.Lac/Ar	Lac.Ar	CFO	Cort.Th
N.On/Ar	1.000								
On.B/Ar	0.930[c]	1.000							
NREs	0.214	0.255[a]	1.000						
On.Ar	0.119	0.266[b]	−0.064	1.000					
Po/Ar	0.169	0.231	0.462[c]	0.060	1.000				
N.Lac/Ar	0.156	0.135	0.049	0.152	0.045	1.000			
Lac.Ar	−0.021	−0.023	0.177[b]	−0.021	0.047[a]	0.355[c]	1.000		
CFO	−0.213	−0.232	−0.129	−0.142	−0.212[b]	−0.386[b]	−0.023	1.000	
Cort.Th	0.561[c]	0.622[c]	0.397[a]	0.213	0.226	0.525[c]	0.007	−0.710[c]	1.000

[a] = $P < 0.05$; [b] = $P < 0.01$; [c] = $P < 0.001$.

TABLE 3B. Correlations: Sub-adult bones (*r* values)

	Po/Ar	N.Lac/Ar	Lac.Ar	CFO	Cort.Th
Po/Ar	1.000				
N.Lac/Ar	0.112	1.000			
Lac.Ar	0.144	0.718[c]	1.000		
CFO	−0.204[a]	−0.581[c]	−0.417	1.000	
Cort.Th	0.119	0.416[b]	0.397[b]	−0.475[c]	1.000

[a] = $P < 0.05$; [b] = $P < 0.01$; [c] = $P < 0.001$.

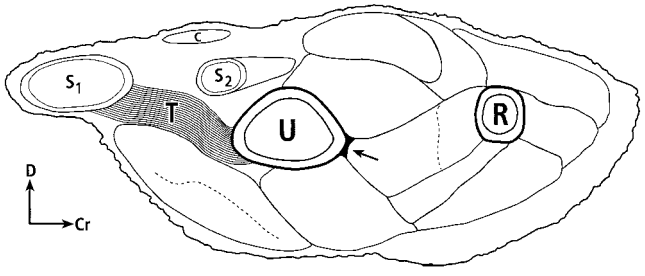

Fig. 10. Proximal-to-distal view of a transverse cross section of a left adult turkey forelimb at mid-diaphysis (U, ulna; R, radius; D, dorsal; Cr, cranial; T, "tether" of secondary feather (S1) sheath; S2, second secondary feather; C, secondary covert feather (the arrow indicates the location where three muscles form a firm coinsertion along the cranial cortex)). The section was made using a wing frozen in full extension. However, the secondary feathers are still oblique to the plane of section (see Fig. 1, middle drawing). The tether (T) and secondary feather sheath form a structure that is broader than the feather tip when viewed from dorsal to ventral. Therefore, the proximal aspect of the tether of S1 is seen clearly in this section; the distal aspect of the tether of S2 is just proximal to the plane of the section. In contrast to the continuous firm coinsertion along the cranial cortex (arrow), the tethers of the 18 secondary feathers insert in relatively discrete locations (i.e., they are not confluent) along the caudal cortex.

Analyses of individual octants and combined locations showed that only the subadult turkey ulnae exhibited regional CFO patterns corresponding to prevalent tension and compression. This presumed strain-mode-related association is consistent with the pattern shown in other "tension" vs. "compression" cortical regions of the bones noted above. It has been suggested that these variations are adaptive, since they can influence toughness, energy absorption, and microcrack propagation in the physiologic context of "strain-mode-specific" loading (i.e., when loading a habitual "tension" cortex in tension, or a habitual "compression" cortex in compression) (Riggs et al., 1993a; Reilly and Currey, 1999, 2000; Shelton et al., 2000; Skedros et al., 2000a, 2001a, b, 2003a, b).

The adult turkey ulnae, however, showed a comparatively more uniform CFO pattern, rather than the expected tension vs. compression distribution. If predominant CFO is truly strain-mode sensitive and specific, then the ulnae of subadult turkeys may experience relatively simpler bending loads compared to adults. Observation of turkey behavior has revealed that subadults flap their wings with much greater frequency and vigor compared to adult animals (D. Adams, personal communication). Consequently, it is suggested that the subadult ulna receives relatively more prevalent bending than adults. In contrast, torsional loading (hence increased shear) may be relatively more prevalent in adults, ultimately producing shear-related adaptations such those shown in the ovine tibia, where CFO patterns also appear relatively uniform throughout an entire diaphyseal cross-section (Skedros, 2001, 2002). Histologic observations are also consistent with this hypothesis (see below). These possibilities warrant further study, especially since experimental data show that functionally equivalent sites in growing and mature weight-bearing limb bones of various species are typically subject to similar in vivo strain histories (e.g., similar strain distributions and principal strain orientations) (Lanyon and Baggott, 1976; Lanyon et al., 1979; Biewener et al., 1986; Keller and Spengler, 1989; Indrekvan et al., 1991; Biewener and Bertram, 1993a; Biewener, 1993).

Implications of regional and age-related histology. In a study involving limb bones of adult mallard ducks, de Margerie (2002) suggested that laminar bone with a predominance of circular primary osteons represents an adaptation for habitual shear stress (e.g., as a result of torsion). He reported that this histology was most prevalent in the torsionally loaded humerus, ulna, and femur. In contrast, bones subjected to habitual bending (e.g., radius, tibiotarsus, tarsometatarsus) exhibited laminar bone with a predominance of oblique and radial pri-

mary osteons. If these relationships between bone histology and habitual loading are correct, then our observations suggest that the histology of the adult turkey ulnae is generally consistent with a habitual torsion environment. In contrast, the histology of subadult turkey ulnae appears generally more consistent with habitual bending. However, in both groups the histology cranial and caudal regions, where shear strains and off-axis (i.e., oblique to the diaphyseal long axis) longitudinal strains predominate, are consistent with habitual shear. Quantification of the degree of "laminarity" (i.e., torsion vs. bending, sensu de Margerie (2002)) and the correlation of this measurement with CFO were not evaluated in the current study.

Osteocyte Lacuna Population Density (N.Lac/Ar) and Lacuna Area (Lac.Ar)

Age-related variations in N.Lac/Ar. Results showed that osteocyte lacuna population densities are 25% greater in immature bones than in mature bones (1,314.9 ± 307.5/mm^2 vs. 1,049.5 ± 184.8/mm^2, respectively, $P < 0.0001$). These values are substantially greater than those reported for some mammalian bones, including cortical bone of mid-diaphyses of human femora (approximately 450–900/mm^2 and 450–700/mm^2 in adolescent-to-elderly adult males and females, respectively) (Vashishth et al., 2000); rabbit femora (approximately 975 ± 300/mm^2; Remaggi et al., 1998); ovine and cervine calcanei (623.7 ± 63.1/mm^2, range: 510.5–732.8 (Hunt and Skedros, 2001; Skedros et al., 2000b)); equine radii and third metacarpals (493.3 ± 93.2/mm^2, range: 404.9–584.6 (Skedros et al., 1996b, 2000c)); and cancellous bone of the human iliac crest biopsies (mean ± S.D. = 182.6 ± 39.9/mm^2, range: 108.6–266.5 (Mullender et al., 1996b)). However, the relatively high N.Lac/Ar in the subadult turkey ulnae is consistent with N.Lac/Ar data reported in cortical bone of mid-diaphyseal chick femora (approximately 1875/mm^2, n = 3) (Marotti et al., 1990; Remaggi et al., 1998) (F. Remaggi, personal communication). The substantially greater N.Lac/Ar value in an avian species may be a function of their relatively higher specific metabolic rate (metabolic rate per kilogram of body mass) (Schmidt-Nielson, 1985). This possibility is supported by limited data from avian and mammalian species that suggest that N.Lac/Ar may be positively correlated with specific metabolic rate and inversely correlated with animal size (Mullender et al., 1996a; Remaggi et al., 1998; Cullinane, 2001, and personal communication).

It is difficult to obtain an "aged" skeleton from a domestic turkey, due to a myriad of age-related morbidities (Rubin et al., 1992, and personal communication). Nevertheless, the significant reduction in N.Lac/Ar reported in the present study is consistent with age-related reductions observed in cortical (Vashishth et al., 2000) and cancellous (Mullender et al., 1996b) bone of human iliac crest biopsies and cortical bone from canine femoral diaphyses (Frank et al., 2002). Several investigators have also demonstrated an age-related decrease in the viability of osteocytes in cortical bone from human femoral heads (Dunstan et al., 1993), human femoral necks (Power et al., 2001), and canine femoral mid-diaphyses (Frank et al., 2002). Although we could not assess osteocyte viability in the present study, it is clear that N.Lac/Ar is not uniform within a cross-section or between age groups.

Feather "tether" insertions and intercortical variations in N.Lac/Ar and osteonal remodeling. Our dissections of mature turkey forelimbs demonstrate that a fibrous "tether" of each secondary feather sheath firmly inserts into the caudal aspect of the ulna cortex (Fig. 10).[2] An additional "firm" fibrous muscle coinsertion occurs along the cranial cortex. Although no bony excrescence is detectable in either location, these locations are where the cortex is thickest in adults. We speculate that stresses applied to these regions, especially along the caudal cortex via the tethers, during wing and feather motion influences the structural and material organization of these regions, resulting from significantly increased remodeling activity (i.e., increased N.On/Ar and NREs, and reduced %ash) and increased N.Lac/Ar in the caudal and ventral-caudal region of adult bones. In view of published strain gauge data (Rubin and Lanyon, 1985), however, the magnitude of the loads imparted to this region via these tethers is unknown. But the contribution of feathers in producing strains in the diaphysis is thought to be highly significant (C.T. Rubin, personal communication).

Nevertheless, the relatively high N.Lac/Ar in the caudal region cannot be simply attributed to locally increased remodeling since relatively lower N.Lac/Ar has been reported in human cancellous bone, which typically remodels faster than cortical bone (Marotti, 1976; Parfitt, 2002). Additionally, osteocyte lacuna densities are relatively lower in the caudal cortex of subadult and adult mule deer calcanei (Skedros et al., 2000b) even though remodeling rates in this region appear to be relatively greater than in the cranial, medial, and lateral cortices (Skedros et al., 1994b, 1997, 2001c). These data and the poor correlation shown in the present study between N.Lac/Ar, N.On/Ar and NREs (all r-values < 0.2) suggest that the relatively increased N.Lac/Ar in the caudal cortex of the adult turkey ulna cannot be attributed to the locally increased remodeling.

Implications for osteocyte function. Since osteocyte lacunae may become stress-risers for the formation of microdamage, especially with age or excessive exercise (Reilly, 2000), and osteocytes may be the "mechano-sensors" of microdamage (Martin, 2002), modifying their concentration may enhance bone's fatigue life and/or other aspects of mechanical behavior (Mullender and Huiskes, 1995; Fyhrie and Vashishth, 2000; Yeni & Fyhrie, 2002). However, regional variations in N.Lac/Ar alone do not consistently correlate with habitual strain mode and magnitude distributions (Skedros et al., 1996a, 2000b, c; Hunt and Skedros, 2001). Although artiodactyl and equine calcanei demonstrate significantly higher N.Lac/Ar in "compression" vs. "tension" cortices (horse: 650 ± 71 vs. 599 ± 110; elk: 732 ± 55 vs. 644 ± 62; and sheep: 710 ± 65 vs. 609 ± 64; $P < 0.05$ for all comparisons), equine third metacarpals have lower N.Lac/Ar in cortical locations habitually loaded in "compression" vs. "tension" (425 ± 77 vs.

[2]The secondary feathers are the largest feathers that insert into the radius-ulna forelimb region. The primary features are associated with bones in the manus (distal to the radius and ulna) (Lucas and Stettenheim, 1972; Proctor and Lynch, 1993).

533 ± 91, $P < 0.001$) (Skedros et al., 2000c). In contrast, equine radii have higher N.Lac/Ar in "compression" vs. "tension" cortices (522 ± 128 vs. 478 ± 138, $P < 0.05$) (Skedros et al., 1996b). Although these small differences in equine radii are statistically significant, the increased distance between any two osteocytes is only about 2 μ and may bear little biomechanical advantage. Additionally, N.Lac/Ar in these two equine bones does not correlate with regional variations in strain magnitude or mode. The present study showed that N.Lac/Ar is not significantly different between "compression" (dorsal) vs. "tension" (ventral) cortices, or between high longitudinal strain (e.g., dorsal) vs. low longitudinal strain (e.g., cranial) cortices in both age groups (Fig. 7). Therefore, it appears that osteocyte density, as estimated from lacuna densities in cortical bone, is not a useful characteristic for interpreting strain history in terms of magnitude and mode. However, N.Lac/Ar may be useful for delineating regional variations in functional strain distribution and/or metabolic activity.

There is evidence that N.Lac/Ar is negatively correlated with microdamage accumulation in cortical bone of the aging human femur at mid-diaphysis (Turner et al., 1998; Reilly, 2000; Vashishth et al., 2000) and canine femur at mid-diaphysis (Frank et al., 2002). This relationship may reflect a failure to repair microdamage, since viable osteocytes are probably necessary for its detection (Martin, 2000, 2002). Selective resorption of bone with relatively more osteocytes (i.e., microdamage "sensors") may eventually lead to bone tissue with relatively lower osteocyte density and an accumulation of microdamage (Mullender et al., 1996b; Vashishth et al., 2000). Additional studies are needed to determine whether such an association exists between microdamage density and osteocyte viability and/or N.Lac/Ar in the developing and aging turkey ulna.

Osteocyte densities and nutritional constraints. Nutrient exchange involving osteocytes (e.g., vascular transport, convective flow, diffusion, etc.) is probably the most important factor limiting variations and changes in the population density of these cells (Mullender and Huiskes, 1997; Knothe Tate and Niederer, 1998; Knothe Tate et al., 1998; Fyhrie and Kimura, 1999; Cullinane, 2001). In the present study, both vascular and nonvascular porosities were highest near the neutral axis sites (i.e., caudal and cranial cortices). These were also the locations where the bone cortex was thickest. These sites may require more blood supply in order to deliver nutrients to cells within the cortex. It is suggested that requirements for nutrient supply and delivery have a role in modulating certain aspects of bone morphology, including N.Lac/Ar and porosity (and hence bone volume fraction) (Mullender and Huiskes, 1997; Cullinane, 2001; Vashishth et al., 2002). The increase in N.Lac/Ar at these sites (in both mature and immature ulnae) may be a consequence of the increased vascular supply required to support the greater bone mass. In turn, the increased cortical thickness in these locations may be strongly influenced by the larger population of osteocytes (Vashishth et al., 2002).

In addition, the adaptive relevance of regional, nonpathologic, and nonsenescent cell population differences suggested by the N.Lac/Ar data shown in the present study is unclear. Such variations, including regional variations in N.On/Ar and On.B/Ar (see further discussion below) may have more to do with variations in growth-related modeling and remodeling drifts than with corresponding characteristics or consequences of regional mechanical loading (Amprino and Sisto, 1946; Smith, 1960; Enlow, 1963; Oyen and Russell, 1982; de Ricqlès et al., 1991; Biewener and Bertram, 1993b; McMahon et al., 1995). These possibilities and the paucity of N.Lac/Ar data in avian bones make it difficult to speculate about advantages of the nonuniform microporosity data reported in the present study. Controlled ontogenetic studies are needed to further examine these issues.

Osteocyte lacuna area (Lac.Ar). The regional variations shown in mean Lac.Ar (Fig. 8) may be influenced by their orientation, since lacunae frequently have ovoid shapes and may be elongated in a preferred direction (Cane et al., 1982; Remaggi et al., 1998). The idea that lacunae orientation and/or size may have regional differences, and may reflect differences in local habitual loading conditions and/or histology is based on several observations: 1) CFO and Lac.Ar are moderately correlated in the present study ($r = -0.471$, $P < 0.01$), and 2) the orientation of osteocyte lacunae in various bone types can be correlated with predominant CFO or collagen packing density (Remaggi et al., 1998; Ferretti et al., 1999; Ardizzoni, 2001; Hunt and Skedros, 2001). For example, correlation analyses between N.Lac/Ar and various microstructural and ultrastructural characteristics in equine third metacarpals have shown that the only r-value exceeding $|0.400|$ was with CFO ($r = 0.408$, $P < 0.001$) (Hunt and Skedros, 2001). Our observations in adult turkey ulnae also suggest that lacuna areas are different in octants where changes in gross histologic patterns are most evident. For example, mean Lac.Ar is highest in the cranial and caudal cortices, where, along with the ventral-caudal cortex, histology differs markedly from the other locations (Figs. 4 and 5). Additional studies are needed to determine whether there are biomechanically important relationships between Lac.Ar and collagen organization and other material characteristics.

Mineral Content (%ash), Secondary Osteon Population Density (N.On/Ar) and Area (On.Ar), Fractional Area of Secondary Bone (On.B/Ar), and Porosity (Po/Ar)

The lack of secondary osteons in immature bones, as well as the absence of correlation between CFO and On/Ar in mature bones, suggests that variations in CFO in these groups are produced by bone modeling (i.e., in the primary bone) and hence are not strongly linked to osteonal remodeling. Apart from predominant CFO, no other structural or material characteristics examined in limb diaphyses of various mammalian species have demonstrated significant differences that are highly specific for the tension/compression strain distribution produced by habitual bending (Skedros, 2001). For example, mechanically important %ash differences occur between the opposing "tension/compression" cortices in ovine, cervine, and equine calcanei (Skedros et al., 1993b, 1994a, 1997, 2001c; Mason et al., 1995), but are minimal or absent in ovine, cervine, and equine radii (Lanyon et al., 1979; Riggs et al., 1993a; Mason et al., 1995; Riches et al., 2000; Skedros et al., 2003c), human femora (Amtmann and Schmitt, 1968; Kimura and Amtmann, 1984), and turkey ulnae (present study). Similarly, data from various "tension/compression" bones lack strain-mode-specific associations of On.B/Ar, N.On/Ar, and osteon cross-sectional area and cross-

sectional shape (Lanyon and Baggott, 1976; Lanyon and Bourn, 1979; Carter et al., 1980, 1981; Bouvier and Hylander, 1996; Gies and Carter, 1982; Martin and Burr, 1989; Skedros et al., 1994b, 1996a, 1997; Mason et al., 1995; Skedros, 2000, 2001).

In view of these findings, it remains unclear whether the regional material heterogeneities in the turkey ulna diaphysis reflect material or structural properties that are mechanically relevant. While local material variations can affect local mechanical behavior, there are apparently no data that unequivocally support the hypothesis that intracortical remodeling is a means of significantly affecting whole-bone flexural (i.e., deformation of the whole bone as a structure) properties in adults. Developmental morphologic changes produced by modeling (e.g., cortical thickness and cross-sectional shape) show the best correlation with these adaptations (Woo et al., 1981; Biewener and Bertram, 1993b; Gross et al., 1992; Les, 1995; Alexander, 1998; Skedros, 2001; Skedros et al., 2003c). In contrast, experimental data show that bone remodeling, via the introduction of secondary osteons, their lamellae, and cement lines, can significantly influence regional toughness, energy absorption, and/or fatigue resistance of cortical bone (Martin et al., 1996b; Reilly et al., 1997; Nunamaker et al., 1987, 1990; Skedros et al., 2003a, b). In turn, greater densities of secondary osteons or On.B/Ar can enhance fatigue resistance and fracture toughness by influencing microcrack propagation at a local level (Reilly et al., 1999; Reilly and Currey, 1997; Shelton et al., 2000). Such adaptation might be expected in the vicinity of the turkey ulna caudal and ventral-caudal cortices, since, as noted above, shear strains are probably more localized in these locations. Since cortical bone is generally weaker in shear than tension or compression, these localized shear strains may be a sufficient stimulus (e.g., by producing microdamage) for causing intracortical resorption and secondary osteon formation. There is increasing evidence for the influence of shear stresses on bone organization in this general context (Rubin et al., 1996; Pidaparti and Turner, 1997; Carter et al., 1998; Su et al., 1999; Turner et al., 2001; Skedros, 2002). Thus, shear stresses may be relatively more important in evoking matrix anisotropy than tension or compression (Norman et al., 1996; Jepsen and Davy, 1997; Yeni et al., 2001).

Matrix Heterogeneity and Fluid Flow

Interstitial fluid through bone matrix, which arises as a result of functional load bearing, has been proposed as a primary mechanism driving modeling and remodeling (Weinbaum et al., 1994; Wang et al., 1999; Srinivasan and Gross, 2000; You et al., 2001). Srinivasan and Gross (2000) recently used an analytical model to examine load-induced canalicular fluid flow in the adult turkey ulna at mid-diaphysis. While these and other investigators who use theoretical models often assume that the bone matrix has a homogeneous material organization (Salzstein et al., 1987; Brown et al., 1990; Knothe Tate and Niederer, 1998; Yeni et al., 2001; Qin et al., 2002, 2003), anisotropic material properties can be important in the turkey ulna for accurate finite element solutions (Ricos et al., 1996; Qin et al., 1998). Results of the present study suggest that accurate analytical models of fluid flow through bone matrix will also require the understanding of local variations in these specific characteristics. The neutral axis regions showed the greatest amount of both "nonvascular" (e.g., osteocyte lacunae) and "vascular" porosity (e.g., primary canals, or central canals of mature or forming secondary osteons). In their analytical model, which assumed regionally uniform lacunae and canalicular dimensions and distributions, Srinivasan and Gross (2000) found that spatio-temporal fluid flows and strain gradients in the circumferential direction are greatest along the neutral axis, where the greatest N.Lac/Ar were found in the present study. In contrast, they showed that spatio-temporal fluid flows in the radial direction are greatest in the "tension" and "compression" cortices; in these regions, we found the greatest Lac.Ar, but relatively lower "vascular" and "nonvascular" porosities. Additionally, data in the present study showing greater "vascular" porosity and larger mean Lac.Ar in the endocortical region compared to the pericortical region suggests a greater capacity for fluid flow through the porosity of the endocortical matrix relative to the pericortex. For analytical models examining the relationships between strains and fluid-flow through the porosity of the adult turkey ulna, it is important to emphasize that these regional variations in lacuna and nonlacuna porosities are not correlated across octant locations.

Local strain and/or fluid-flow patterns may not be linked in an obvious, straightforward fashion. For example, although magnitudes of longitudinal strains are low in neutral axis regions, matrix and extravascular fluid flow and strain gradients are typically high in these regions (Gross et al., 1997; Srinivasan and Gross, 2000). Significant differences in fluid-flow dynamics can occur through the porosities of tension, compression, and shear regions of a functionally or experimentally loaded bone diaphysis (McDonald and Pitt Ford, 1993; Gross et al., 1997; Judex et al., 1997; Srinivasan and Gross, 2000; Knothe Tate et al., 2000). Maximal fluid displacements typically occur in the proximity of the neutral axis of bending (Steck et al., 2000; Qin et al., 2001). Regional ultra- and microstructural heterogeneities may influence these local fluid-flow patterns (Wang et al., 1999; Qiu et al., 2001; Qin et al., 1999, 2002). The roles that various types of porosities (e.g., vascular channels, lacunar-canalicular spaces, and collage-apatite spaces) and structural/material anisotropies have in affecting fluid flow are important considerations since there is mounting evidence suggesting that: 1) osteocytes experience significant shear stress and/or streaming potentials from load-induced fluid flow into lacunar-canalicular spaces (McLeod et al., 1998; Weinbaum et al., 1994; You et al., 2001; Pollack, 2001), 2) osteocytes are more sensitive to fluid flow due to mechanical loading than to the deformation of the mineralized tissue (Owan et al., 1997; Smalt et al., 1997; Su et al., 1997; Jacobs et al., 1998; You et al., 2000, 2001), and 3) local patterns of fluid flow may regulate the coupling of osteoblasts and osteoclasts in the formation and migration of a developing secondary osteon (Robling and Stout, 1999; Smit and Burger, 2000; Smit et al., 2002).

Cross-Sectional Geometry, Cortical Thickness, Interosseous Radius-to-Ulna Distance, and Diaphyseal Curvature: Implications for Regional Modeling and Cortical Drift

According to Rubin and Lanyon (1985), the turkey ulna models during growth predominantly by uniform endosteal resorption and periosteal apposition. However,

quantitative data describing this process throughout ontogeny have not been reported (S.P. Fritton and S.D. Bain, personal communication). Several measurements made in the present study can be used to infer general patterns of modeling drifts.

Although there were no significant differences in the orientation of Imax (Φ angle) between the age groups (immature 7.7° vs. mature 5.3°, $P = 0.19$), the ratio of Imax/Imin increased with age (immature = 1.31 vs. mature = 1.47, $P < 0.05$). Thus it appears that in the age interval studied, the cranial-caudal axis (the predominant neutral axis during functional loading) increases in cortical thickness, resulting in a greater influence on the moment of inertia (Imax) than to that along the orthogonal (dorsal-ventral) axis. However, the overall cortical area did not change relative to the total cross-sectional area. It therefore seems unlikely that both bones would drift in the cranial or caudal direction, since gross curvature does not change in these directions.

At mid-diaphysis the cross-sectional shape of the turkey ulna may enhance loading predictability by allowing bending to occur preferentially along the dorsal-ventral axis (Bertram and Biewener, 1988). This may also be enhanced by sagittal curvature, which is most prominent in the dorsal-ventral direction. Robust cortices along the cranial-caudal axis may, in turn, minimize bending along the cranial-caudal axis. Similar (but more dramatic) relationships between habitual bending and curvature/cross-sectional shape have been described in equine and sheep radii (Lanyon et al., 1979; Riggs et al., 1993b). However, in contrast to these bones, the adult turkey ulnae have a relatively smaller Imax/Imin ratio. This suggests a comparatively more annular shape, consistent with adaptation expected in a torsional environment (Wainwright et al., 1982; Currey and Alexander, 1985). Thus, the turkey ulna appears to be constructed for both bending and torsion.

The results of our microscopic analyses and cortical thickness measurements suggest that adult bones do not contain residual bone from the subadult stage. This may indicate that the cross section increases in size around a centroid that maintains the same relative position in three-dimensional space, and that bone is uniformly removed from endosteal surfaces. However, the age-related increase in thickness of the caudal cortex relative to the other cortices suggests that the ulna tends to model in the caudal direction. Additional studies using fluorochrome labels in a series of growing animals are needed to clarify these putative modeling dynamics.

Structural/material compensation and scaling relationships. The adult bones have significantly higher BSIs than the subadult specimens (Table 1). This difference is more strongly affected by differences in section modulus (Z) than bone length. Furthermore, there are moderate correlations between BSI and both whole-bone %ash and CFO, and the correlation with CFO is strongest in subadults (Table 2). It is plausible that some material characteristics (e.g., CFO) in subadult turkeys may compensate for their lower strength. The idea that a bone's structural and material characteristics can work in a compensatory fashion has been suggested by studies of bones of various species (Martin and Atkinson, 1977; Martin et al., 1980; Burr et al., 1990; Lieberman and Crompton, 1998; Pearson and Lieberman, 2002). The most convincing appears to be Carrier's (1983) data from an ontogenetic series of jack rabbits (*Lepus californicus*). Carrier examined changes in material constitution (i.e., ash content) and structural organization (i.e., the second moment of area, I) in the metatarsal and femur, and noted that I is relatively larger in young animals than adults. This relationship was illustrated by a negative allometry between body mass and I for these bones. Carrier (1983, p. 47) speculated that "[t]he large second moment of area in young hares will reduce the stress that the bone tissue experiences, and thus act to compensate for the low mineralization and intolerance to stress observed in juvenile bone tissue." The notion of extrapolating this idea to the developing turkey ulna is compelling, since that bone may exhibit a similar capacity for structural/material compensation. However, we are hampered by our inability to determine how ash content, CFO, or other material characteristics change as a function of body mass or muscle contraction force (these data were not available).

In addition, geometric scaling relationships between avian long bones of hind limbs and wings can dramatically differ. In their study of skeletal growth in sea gulls, Carrier and Leon (1990) showed that during post-hatching growth, the mid-diaphysis of hind-limb bones (femur, tibia, metatarsus) remains isometric or undergoes strong negative allometry with respect to body mass, while the mid-diaphysis of wing bones (humerus, ulna, metacarpus) undergoes strong positive allometry, becoming relatively thicker. Similar scaling relationships may occur during the growth of the domestic turkey. Consequently, Carrier's idea of structural/material compensation may not be directly applicable in the avian wing. Nonetheless, it is plausible that the apparent bending-related CFO patterns and/or generally more longitudinal CFO in subadult turkey ulnae may represent material compensation for their lower BSIs (Table 2). Mechanical testing, correlated with structural and material characteristics, would be necessary to determine whether these correlations represent significant adaptations.

SUMMARY AND CONCLUSIONS

The results of this study show regional micro- and ultrastructural heterogeneities in the turkey ulna at mid-diaphysis. In adult bones, the lowest mineral content and more robust cortical thickness occurred in the ventral-caudal and caudal cortices. It may not be coincidental that shear strains are also generally highest in these regions. Structural variations were relatively minor in the age interval studied, whereas regional material variations varied substantially. Only subadult bones exhibited non-uniform CFO patterns corresponding to prevalent tension (ventral) and compression (dorsal). These variations may be adaptations for differential mechanical requirements in "strain-mode-specific" loading. In contrast, the more uniform oblique-to-transverse CFO patterns in adult bones may represent adaptations for shear strains produced by habitual torsional loading, which may be more prevalent in adults. There is evidence of structural adaptation for both bending and torsion in both age groups.

Regional variations in lacunar ("nonvascular") and non-lacunar ("vascular") porous spaces are present in the turkey ulna at mid-diaphysis. In adult bones, the greater nonlacunar porosity and larger mean lacuna area in the endocortical region compared to the pericortical region suggests a capacity for a greater volume of fluid flow

through the porous spaces of the endocortical matrix. Significant regional microstructural heterogeneity—specifically, greater N.Lac/Ar, Lac.Ar, and Por/Ar (and N.On/Ar in adults)—also occurs in the cortices along the neutral axis. This may influence both fluid flow and strain characteristics that are known to occur along this axis. Regional variations in lacuna and nonlacunar porosities are not correlated in adult bones. These are important considerations in the context of analytical and computational models that examine the relationship between strains and fluid-flow through the various matrix porosities. Regional micro- and ultrastructural heterogeneities may influence strain/fluid-flow dynamics, which are considered proximate influences in bone development, adaptation, and maintenance.

ACKNOWLEDGMENTS

The authors thank Roy Bloebaum, Kent Bachus, and the Salt Lake City Veterans Administration Bone and Joint Research Laboratory for providing some of the technical equipment and support used for this study; Pat Campbell and Harlan Amstutz for the use of their laboratory facilities at the Joint Replacement Institute of Orthopaedic Hospital in Los Angeles, California; and Clinton T. Rubin for providing some of the bones used in this study. We thank Christian Sybrowsky, Barr Peterson, Cameron Bevan, and Alex Millet for their technical work, and Kerry S. Matz for the illustrations. This research was funded by the Doctors' Education and Research Fund at Orthopaedic Hospital in Los Angeles, CA; the Department of Veterans Affairs Medical Center, Salt Lake City, UT; and the Utah Osteoporosis Center, Salt Lake City, UT.

APPENDIX A

Definitions

Adaptation. Adaptation in cortical bone commonly refers to either 1) changes in bone structure and/or material organization in response to loading conditions outside a normal physiologic stress/strain range, distribution, and/or duration (e.g., Lanyon et al., 1979; Woo et al., 1981; Currey, 1984; Schaffler et al., 1985; Martin and Burr, 1989; Biewener and Bertram, 1994), or 2) the presence of regional differences in structural and/or material organization that are strongly influenced by normal functional stimuli occurring during normal development within or between bones (e.g., Currey, 1984; Martin and Burr, 1989; Bertram and Swartz, 1991; Riggs et al., 1993a, b; Skedros et al., 1994a, b). In the present investigation, "adaptations" are considered to be biomechanically relevant regional variations and temporal changes in cortical bone structural and material organization that are produced by the modeling and remodeling processes during normal skeletal development. In addition to being mediated by genetic and epigenetic influences, which are heritable, these processes may be influenced by nonheritable ("extragenetic") stimuli, such as regional variations in microdamage incidence.

Modeling. Adaptations resulting from modeling activities include the accretion and/or resorption of secondary or nonsecondary bone (e.g., circumferential lamellae, and trabecular bone in some cases) on periosteal or endosteal surfaces. They are detected as changes and/or differences in a bone's curvature, cross-sectional shape, and/or regional cortical thickness. Consequently, modeling is a concept describing a combination of nonproximate, though coordinated, resorption and formation drifts, the net result of which is to change the distribution of bone (Jee et al., 1991). Such drifts are called macro-modeling in cortical bone, and mini-modeling in cancellous bone (Frost, 1988a, b). The generic term "modeling" is used herein to describe growth-related macro-modeling.

Remodeling. Adaptations produced by remodeling activities involve the replacement of intracortical bone. This is achieved through the activation of basic multicellular units (BMUs) that create secondary osteons (Haversian systems) in cortical bone (Frost, 1986; Jee et al., 1991; Parfitt et al., 1996). Manifestations of remodeling adaptations include regional changes and/or differences in secondary osteon population density (N.On/Ar), fractional area of secondary bone (On.B/Ar), cross-sectional area of individual secondary osteons (On.Ar), and/or porosity. If a bone has increased On.B/Ar, then the bone is more "remodeled." In contrast, "remodeling" connotes an active renewal process (Parfitt et al., 1996). Remodeling rates are thought to be the primary determinant of mineralization differences in the bone matrix within the cortices of many bones (Grynpas, 1993; Martin, 1993). A relatively increased remodeling rate in a region of bone is detected in the present investigation as relatively decreased bone matrix mineral content, and increased population densities of resorption spaces and newly forming secondary osteons (Skedros et al., 1997).

APPENDIX B

Abbreviations

CFO = predominant collagen fiber orientation expressed as WMGL (see below).
Cort.Th = cortical thickness (mm).
Imax = major axis of second moment of area (mm^4).
Imin = minor axis of second moment of area (mm^4).
J = polar moment of inertia (mm^4).
Lac.Ar = mean cross-sectional area of osteocyte lacunae (μm^2).
N.Lac/Ar = osteocyte lacuna population density (no./mm^2).
N.On/Ar = secondary osteon population density (no./mm^2).
NREs = new remodeling events (resorption spaces plus newly forming osteons) (no./mm^2).
On.Ar = average area of secondary osteons (mm^2).
On.B/Ar = fractional area of secondary osteonal bone $\times$ 100 (%).
Po/Ar = fractional area of nonlacunar porous spaces $\times$ 100 (%).
WMGL = weighted mean gray level. Larger numbers indicate more oblique-to-transverse collagen; smaller numbers indicate more longitudinal collagen (see CFO above).
%Ash = mineral content.

LITERATURE CITED

Adams DJ, Spirt AA, Brown TD, Fritton SP, Rubin CT, Brand RA. 1997. Testing the daily stress stimulus theory of bone adaptation with natural and experimentally controlled strain histories. J Biomech 30:671–678.

Alexander RM. 1998. Symmorphosis and safety factors. In: Weibel ER, Taylor CR, Bolis L, editors. Principles of animal design: the optimization and symmorphosis debate. Cambridge, UK: Cambridge University Press. p 28–35.

Amprino R, Sisto L. 1946. Analogies et différences de structure dans les différentes régions d'un mème os. Acta Anat 2:202–214.

Amtmann E, Schmitt HP. 1968. On the distribution of cortex density in the human femoral shaft and its significance for the determination of bone consistency. Z Anat Entwicklungsgesch 127:24–41.

Ardizzoni A. 2001. Osteocyte lacunar size-lamellar thickness relationships in human secondary osteons. Bone 28:215–219.

Ascenzi A, Boyde A, Portigliatti Barbos M, Carando S. 1987. Microbiomechanics vs. macro-biomechanics in cortical bone. A mechanical investigation of femurs deformed in bending. J Biomech 20: 1045–1053.

Bertram JEA, Swartz SM. 1991. The 'law of bone transformation': a case of crying Wolff? Biol Rev 66:245–273.

Bertram JEA, Biewener AA. 1988. Bone curvature: sacrificing strength for load predictability? J Theor Biol 131:75–92.

Biewener AA. 1993. Safety factors in bone strength. Calcif Tissue Int 53:S68–S74.

Biewener AA, Bertram JEA. 1993a. Skeletal strain patterns in relation to exercise training during growth. J Exp Biol 185:51–69.

Biewener AA, Bertram JEA. 1993b. Mechanical loading and bone growth *in vivo*. In: Hall BK, editor. Bone. Vol. VII. Bone growth, part B. Boca Raton, FL: CRC Press. p 1–36.

Biewener AA, Bertram JEA. 1994. Structural response of growing bone to exercise and disuse. J Appl Physiol 76:946–955.

Biewener AA, Swartz SM, Bertram JEA. 1986. Bone modeling during growth: dynamic strain equilibrium in the chick tibiotarsus. Calcif Tissue Int 39:390–395.

Boskey AL, Wright TM, Blank RD. 1999. Collagen and bone strength. J Bone Miner Res 14:330–335.

Bouvier M, Hylander WL. 1996. The mechanical or metabolic function of secondary osteonal bone in the monkey *Macaca fascicularis*. Archs Oral Biol 41:941–950.

Brown TD, Pedersen DR, Gray ML, Brand RA, Rubin CT. 1990. Toward an identification of mechanical parameters initiating periosteal remodeling: a combined experimental and analytic approach. J Biomech 23:893–905.

Burger EH, Klein-Nulend J. 1999. Mechanotransduction in bone—role of the lacunocanalicular network. FASEB J 13(Suppl):S101–S112.

Burr DB, Ruff CB, Thompson DD. 1990. Patterns of skeletal histologic change through time: comparison of an archaic native American population with modern populations. Anat Rec 226:307–313.

Cane V, Marotti G, Volpi G, Zaffe D, Palazzini S, Romaggi F, Muglia MA. 1982. Size and density of osteocyte lacunae in different regions of long bones. Calcif Tissue Int 34:558–563.

Carando S, Portigliatti Barbos M, Ascenzi A, Boyde A. 1989. Orientation of collagen in human tibial and fibula shaft and possible correlation with mechanical properties. Bone 10:139–142.

Carando S, Portigliatti Barbos M, Ascenzi A, Riggs CM, Boyde A. 1991. Macroscopic shape of and lamellar distribution within, the upper limb shafts, allowing inferences about mechanical properties. Bone 12:265–269.

Carrier DR. 1983. Postnatal ontogeny of the musculo-skeletal system in the black-tailed jack rabbit (*Lepus californicus*). J Zool Lond 201:27–55.

Carrier DR, Leon LR. 1990. Skeletal growth and function of the California gull (*Larus californicus*). J Zool Lond 222:375–389.

Carter DR, Smith DJ, Spengler DM, Daly CH, Frankel VH. 1980. Measurements and analysis of *in vivo* strains on the canine radius and ulna. J Biomech 13:27–38.

Carter DR, Caler WE, Spengler DM, Frankel VH. 1981. Uniaxial fatigue of human cortical bone. The influence of tissue physical characteristics. J Biomech 14:461–470.

Carter DR, Beaupré GS, Giori NJ, Helms JA. 1998. Mechanobiology of skeletal regulation. Clin Orthop Relat Res 355(Suppl):S41–S55.

Cullinane DM. 2001. The role of osteocytes in bone regulation: mineral homeostasis versus mechanoreception. J Musculoskeletal Neuronal Interact 2:90.

Currey JD. 1984. The mechanical adaptations of bones. Princeton, NJ: Princeton University Press. 294 p.

Currey JD, Alexander R McN. 1985. The thickness of the walls of tubular bones. J Zool Lond (A) 206:453–468.

de Margerie E. 2002. Laminar bone as an adaptation to torsional loads in flapping flight. J Anat 2016:521–526.

de Ricqlès A, Meunier FJ, Castanet L, Francillon-Vieillot H. 1991. Comparative microstructure of bone. In: Hall BK, editor. Bone. Vol. III. Boca Raton, FL: CRC Press. p 1–78.

Doden E. 1987. Zur strukturellen variation der langen skeletelemente der hand als greif- und/oder lokomotionsorgan Referat. Verh Anat Ges 81:253–269.

Dunstan CR, Lauren PD, Somers NM, Evans RA. 1993. Measurement of osteoclasts and bone resorption by automated image analysis. J Bone Miner Res 8:139–145.

Enlow DH. 1963. Principles of bone remodeling. Springfield, IL: Charles C. Thomas Publishing. p 1–131.

Ferretti M, Muglia MA, Remaggi F, Cane V, Palumbo C. 1999. Histomorphometric study on the osteocyte lacuno-canalicular network in animals of different species. II. Parallel-fibered and lamellar bones. Ital J Anat Embryol 104:121–131.

Frank JD, Ryan M, Kalscheur VL, Ruaux-Mason CP, Hozak RR, Muir P. 2002. Aging and accumulation of microdamage in canine bone. Bone 30:201–206.

Fritton SP, Rubin CT. 2001. *In vivo* measurement of bone deformations using strain gauges. In: Cowin SC, editor. Bone mechanics handbook. 2nd ed. Boca Raton, FL: CRC Press. p 8.1–8.41.

Fritton SP, McLeod KJ, Rubin CT. 2000. Quantifying the strain history of bone: spatial uniformity and self-similarity of low-magnitude strains. J Biomech 33:317–325.

Frost HM. 1986. Intermediary organization of the skeleton. Vol. 1. Boca Raton, FL: CRC Press. 365 p.

Frost HM. 1988a. Structural adaptations to mechanical usage. A proposed "three-way rule" for bone modeling. Part I. Vet Comp Orthop Traumatol 1:7–17.

Frost HM. 1988b. Structural adaptations to mechanical usage. A proposed "three-way rule" for bone modeling. Part II. Vet Comp Orthop Traumatol 2:80–85.

Fyhrie DP, Kimura JH. 1999. NACOB presentation keynote lecture. Cancellous bone biomechanics. North American Congress on Biomechanics. J Biomech 32:1139–1148.

Fyhrie DP, Vashishth D. 2000. Bone stiffness predicts strength similarly for human vertebral cancellous bone in compression and for cortical bone in tension. Bone 26:73–169.

Gies AA, Carter DR. 1982. Experimental determination of whole long bone sectional properties. J Biomech 15:297–303.

Gross TS, McLeod KJ, Rubin CT. 1992. Characterizing bone strain distributions *in vivo* using three triple rosette strain gauges. J Biomech 25:1081–1087.

Gross TS, Edwards JL, McLeod KJ, Rubin CT. 1997. Strain gradients correlate with sites of periosteal bone formation. J Bone Miner Res 12:982–988.

Grynpas M. 1993. Age and disease-related changes in the mineral of bone. Calcif Tissue Int 53(Suppl):S57–S64.

Heinrich RE, Ruff CB, Adamczewski JZ. 1999. Ontogenetic changes in mineralization and bone geometry in the femur of muskoxen (*Ovibos moschatus*). J Zool Lond 247:215–223.

Hinkle DE, Wiersma W, Jurs WG. 1979. Applied statistics for the behavioral sciences. Chicago, IL: Rand McNally College Publishing Co. p 84–85.

Hodges ERS. 1989. Guild handbook of scientific illustration. New York: Van Nostrand Reinhold. p 341–343.

Hunt KJ, Skedros JG. 2001. The role of osteocyte lacunae populations in interpreting loading history of bone. Am J Phys Anthrop 32(Suppl):83.

Indrekvan K, Husby OS, Gjerdet NR, Engesaeter LB, Langeland N. 1991. Age-dependent mechanical properties of rat femur. Measured *in vivo* and *in vitro*. Acta Orthop Scand 62:248–252.

Jacobs CR, Yellowley CE, Davis BR, Zhou Z, Cimbala JM, Donahue HJ. 1998. Differential effect of steady versus oscillating flow on bone cells. J Biomech 31:969–976.

Jee WSS, Li XJ, Ke HZ. 1991. The skeletal adaptation to mechanical usage in the rat. Cells Mater (Suppl) 1:131–142.

Jepsen KJ, Davy DT. 1997. Comparison of damage accumulation measures in human cortical bone. J Biomech 30:891–894.

Judex S, Gross TS, Zernicke RF. 1997. Strain gradients correlate with sites of exercise-induced bone-forming surfaces in the adult skeleton. J Bone Miner Res 12:1737–1745.

Kachigan SK. 1986. Statistical analysis: an interdisciplinary introduction to univariate & multivariate methods. New York: Radius Press. 589 p.

Kalmey JK, Lovejoy CO. 2002. Collagen fiber orientation in the femoral necks of apes and humans: do their histological structures reflect differences in locomotor loading? Bone 312:327–332.

Keller TS, Spengler DM. 1989. Regulation of bone stress and strain in the immature and mature rat femur. J Biomech 22:1115–1127.

Kimura T, Amtmann E. 1984. Distribution of mechanical robustness in the human femoral shaft. J Biomech 17:41–46.

Knothe Tate ML, Knothe U, Niederer P. 1998. Experimental elucidation of mechanical load-induced fluid flow and its potential role in bone metabolism and function adaptation. Am J Med Sci 34:189–195.

Knothe Tate ML, Niederer P. 1998. A theoretical FE-based model developed to predict the relative contribution of convective and diffusive transport mechanisms for the maintenance of local equilibria within cortical bone. Advances in heat and mass transfer in biotechnology. HTD-362/BED-40:133–142.

Knothe Tate ML, Steck R, Forwood MR, Niederer P. 2000. *In vivo* demonstration of load-induced fluid flow in the rat tibia and its potential implications for processes associated with functional adaptation. J Exp Biol 203:2737–2745.

Lanyon LE, Baggott DG. 1976. Mechanical function as an influence on the structure and form of bone. J Bone Joint Surg 58-B:436–443.

Lanyon LE, Bourn S. 1979. The influence of mechanical function on the development and remodeling of the tibia: an experimental study in sheep. J Bone Joint Surg 61A:263–273.

Lanyon LE. 1987. Functional strain in bone tissue as an objective, and controlling stimulus for adaptive bone remodelling. J Biomech 20: 1083–1093.

Lanyon LE, Magee PT, Baggott DG. 1979. The relationship of functional stress and strain to the processes of bone remodelling: an experimental study on the sheep radius. J Biomech 12:593–600.

Les CM. 1995. Material heterogeneity in the equine metacarpus: documentation and biomechanical consequences. Ph.D. dissertation, University of California–Davis, Davis, CA.

Lieberman DE, Crompton AW. 1998. Responses of bone to stress: constraints on symmorphosis. In: Weibel ER, Taylor CR, Bolis L, editors. Principles of animal design: the optimization and symmorphosis debate. Cambridge: Cambridge University Press. p 78–86.

Lucas AM, Stettenheim PR. 1972. Avian anatomy: integument. Part I. Washington, D.C.: U.S. Government Printing Office. 340 p.

Marotti G. 1976. Map of bone formation rate values throughout the skeleton of the dog. In: Proceedings of the 1st workshop on bone morphometry. Ottawa: Ottawa University Press. p 202–207.

Marotti G, Cane V, Palazzini S, Palumbo C. 1990. Structure–function relationships in the osteocyte. Ital J Miner Electrolyte Metab 4:93–106.

Marotti G. 1996. The structure of bone tissues and the cellular control of their deposition. Ital J Anat Embryol 101:25–79.

Martin RB, Atkinson PJ. 1977. Age and sex-related changes in the structure and strength of the human femoral shaft. J Biomech 10:223–231.

Martin RB, Pickett JC, Zinaich S. 1980. Studies of skeletal remodeling in aging men. Clin Orthop 149:268–282.

Martin RB, Burr DB. 1989. Structure, function and adaptation of compact bone. New York: Raven Press. 275 p.

Martin RB, Ishida J. 1989. The relative effects of collagen fiber orientation, porosity, density, and mineralization on bone strength. J Biomech 22:419–426.

Martin RB. 1993. Aging and strength of bone as a structural material. Calcif Tissue Int 53(Suppl 1):S34–S40.

Martin RB, Mathews PV, Lau ST, Gibson VA, Stover SM. 1996a. Use of circularly vs. plane polarized light to quantify collagen fiber orientation in bone. Trans Orthop Res Soc 21:606.

Martin RB, Mathews PV, Lau ST, Gibson VA, Stover SM. 1996b. Collagen fiber organization is related to mechanical properties and remodeling in equine bone. A comparison of two methods. J Biomech 29:1515–1521.

Martin RB. 2000. Does osteocyte formation cause the nonlinear refilling of osteons? Bone 26:71–78.

Martin RB. 2002. Is all cortical bone remodeling initiated by microdamage? Bone 30:8–13.

Mason MW, Skedros JG, Bloebaum RD. 1995. Evidence of strain-mode-related cortical adaptation in the diaphysis of the horse radius. Bone 17:229–237.

McDonald F, Pitt Ford TR. 1993. Blood flow changes in the tibia during external loading. J Orthop Res 11:36–48.

McLeod KJ, Rubin CT, Otter MW, Qin YX. 1998. Skeletal cell stresses and bone adaptation. Am J Med Sci 316:176–183.

McMahon JM, Boyde A, Bromage TG. 1995. Pattern of collagen fiber orientation in the ovine calcaneal shaft and its relation to locomotor-induced strain. Anat Rec 242:147–158.

Mullender MG, Huiskes R. 1995. Proposal for the regulatory mechanism of Wolff's law. J Orthop Res 13:503–512.

Mullender MG, Huiskes R, Versleyen H, Buma P. 1996a. Osteocyte density and histomorphometric parameters in cancellous bone of the proximal femur in five mammalian species. J Orthop Res 14: 972–979.

Mullender MG, van der Meer DD, Huiskes R, Lips P. 1996b. Osteocyte density changes in aging and osteoporosis. Bone 18:109–113.

Mullender MG, Huiskes R. 1997. Osteocytes and bone lining cells: which are the best candidates for mechano-sensors in cancellous bone? Bone 20:527–532.

Nagurka ML, Hayes SC. 1980. An interactive graphics package for calculating cross-sectional properties of complex shapes. J Biomech 13:59–64.

Norman TL, Nivargikar SV, Burr DB. 1996. Resistance to crack growth in human cortical bone is greater in shear than in tension. J Biomech 29:1023–1031.

Nunamaker DM, Butterweck DM, Black J. 1987. Fatigue fractures in thoroughbred racehorses: relationship with age and strain. Trans Orthop Res Soc 12:72.

Nunamaker DM, Butterweck DM, Provost MT. 1990. Fatigue fractures in thoroughbred racehorses: relationships with age, peak bone strain, and training. J Orthop Res 8:604–611.

Ohman JC, Lovejoy CO. 2001. The shape of a long bone's shaft: bending stress or growth plate form? Am J Phys Anthrop 32(Suppl): 115.

Owan I, Burr DB, Turner CH, Qiu J, Tu Y, Onyia JE, Duncan RL. 1997. Mechanotransduction in bone: osteoblasts are more responsive to fluid forces than mechanical strain. Am J Physiol Cell Physiol 273:C810–C815.

Oyen OJ, Russell MD. 1982. Histogenesis of the craniofacial skeleton and models of facial growth. In: McNamara Jr JA, Carlson DS, Ribbens KA, editors. The effect of surgical intervention on craniofacial growth. Monograph no. 12, craniofacial growth series. Ann Arbor, MI: Center for Human Growth and Development, University of Michigan. p 361–372.

Parfitt AM, Mundy GR, Roodman GD, Hughes DE, Boyce BF. 1996. A new model for the regulation of bone resorption, with particular reference to the effects of bisphosphonates. J Bone Miner Res 11: 150–159.

Parfitt AM. 2002. Misconceptions 2: turnover is always higher in cancellous than in cortical bone. Bone 30:807–809.

Pearson O, Lieberman D. 2002. Effects of age and exercise on long bone modeling and remodeling. Am J Phys Anthropol 34(Suppl): 123.

Pidaparti RMV, Turner CH. 1997. Cancellous bone architecture: advantages of nonorthogonal trabecular alignment under multidirectional loading. J Biomech 30:979–983.

Pollack SR. 2001. Streaming potentials in bone. In: Cowin SC, editor. Bone mechanics handbook. 2nd ed. Boca Raton, FL: CRC Press. p 24.1–24.22.

Portigliatti Barbos M, Bianco P, Ascenzi A. 1983. Distribution of osteonic and interstitial components in the human femoral shaft with reference to structure, calcification and mechanical properties. Acta Anat 115:178–186.

Portigliatti Barbos M, Bianco P, Ascenzi A, Boyde A. 1984. Collagen orientation in compact bone: II. Distribution of lamellae in the whole of the human femoral shaft with reference to its mechanical properties. Metab Bone Dis Relat Res 5:309–315.

Power J, Noble BS, Loveridge N, Bell KL, Rushton N, Reeve J. 2001. Osteocyte lacunar occupancy in the femoral neck cortex: an association with cortical remodeling in hip fracture cases and controls. Calcif Tissue Int 69:13–19.

Proctor NS, Lynch PJ. 1993. Manual of ornithology: avian structure & function. New Haven, CT: Yale University Press. 340 p.

Puustjarvi K, Nieminen J, Rasanen T, Hyttinen M, Helminen HJ, Kroger H, Huuskonen J, Alhava E, Kovanen V. 1999. Do more highly organized collagen fibrils increase bone mechanical strength in loss of mineral density after one-year running training? J Bone Miner Res 14:321–329.

Qin L, Mak AT, Cheng CW, Hung LK, Chan KM. 1999. Histomorphological study on pattern of fluid movement in cortical bone in goats. Anat Rec 255:380–387.

Qin Y-X, Rubin CT, McLeod KJ. 1998. Nonlinear dependence of loading intensity and cycle number in the maintenance of bone mass and morphology. J Orthop Res 16:482–489.

Qin Y-X, Cute M, Rubin CT. 2001. The relationship between bone fluid flow and adaptation as stimulated by intramedullary hydraulic loading. Trans Orthop Res Soc 26:319.

Qin Y-X, Lin W, Rubin CT. 2002. The pathway of bone fluid flow as defined by *in vivo* intramedullary pressure and streaming potential measurements. Ann Biomed Eng 30:693–702.

Qiu S, Palnitkar S, Rao D. 2001. Observation on interstitial fluid flow in the lacunar-canalicular network. J Bone Miner Res 16(Suppl 1):S240.

Reilly GC, Currey JD, Goodship AE. 1997. Exercise of young thoroughbred horses increases impact strength of the third metacarpal bone. J Orthop Res 15:862–868.

Reilly GC, Currey JD. 1999. The development of microcracking and failure in bone depends on the loading mode to which it is adapted. J Exp Biol 202:543–552.

Reilly GC. 2000. Observations of microdamage around osteocyte lacunae in bone. J Biomech 33:1131–1134.

Reilly GC, Currey JD. 2000. The effects of damage and microcracking on the impact strength of bone. J Biomech 33:337–343.

Remaggi F, Cane V, Palumbo C, Ferretti M. 1998. Histomorphometric study on the osteocyte lacuno-canalicular network in animals of different species. I. Woven-fibered and parallel-fibered bones. Ital J Anat Embryol 103:145–155.

Riches PE, Everitt NM, McNally DS. 2000. Knoop microhardness anisotropy of ovine radius. J Biomech 33:1551–1557.

Ricos V, Pedersen DR, Brown TD, Ashman RB, Rubin CT, Brand RA. 1996. Effects of anisotropy and material axis registration on computed stress and strain distributions in the turkey ulna. J Biomech 29:261–267.

Riggs CM, Vaughan LC, Evans GP, Lanyon LE, Boyde A. 1993a. Mechanical implications of collagen fibre orientation in cortical bone of the equine radius. Anat Embryol 187:239–248.

Riggs CM, Lanyon LE, Boyde A. 1993b. Functional associations between collagen fibre orientation and locomotor strain direction in cortical bone of the equine radius. Anat Embryol 187:231–238.

Robling AG, Stout SD. 1999. Morphology of the drifting osteon. Cells Tissues Organs 164:192–204.

Rubin CT, Lanyon LE. 1985. Regulation of bone mass by mechanical strain magnitude. Calcif Tiss Int 37:411–417.

Rubin CT, Lanyon LE. 1987. Osteoregulatory nature of mechanical stimuli: function as a determinant of adaptive remodeling in bone. J Orthop Res 5:300–310.

Rubin CT, McLeod KJ, Lanyon LE. 1989. Prevention of osteoporosis by pulsed electromagnetic fields. J Bone Joint Surg Am 71A:411–417.

Rubin CT, Bain SD, McLeod KJ. 1992. Suppression of the osteogenic response in the aging skeleton. Calcif Tissue Int 50:306–313.

Rubin CT, Gross TS, McLeod KJ, Bain SD. 1995. Morphologic stages in lamellar bone formation stimulated by a potent mechanical stimulus. J Bone Miner Res 10:488–495.

Rubin CT, McLeod KJ. 1996. Inhibition of osteopenia by biophysical intervention. In: Marcus R, Feldman D, Kelsey J, editors. Osteoporosis. New York: Academic Press. p 351–371.

Rubin CT, Gross T, Qin YX, Fritton S, Guilak F, McLeod K. 1996. Differentiation of the bone-tissue remodeling response to axial and torsional loading in the turkey ulna. J Bone Joint Surg 78A:1523–1533.

Ruff CB. 1981. Structural changes in the lower limb bones with aging at Pecos Pueblo. Ph.D. dissertation, University of Philadelphia, Philadelphia, PA.

Ruff CB, Hayes WC. 1983. Cross-sectional geometry of Pecos Pueblo femora and tibiae—a biomechanical investigation: I. Method and general patterns of variation. Am J Phys Anthropol 60:359–381.

Ruff CB. 1989. New approaches to structural evolution of limb bones in primates. Folia Primatol 53:142–159.

Salzstein RA, Pollack SR, Mak AF, Petrov N. 1987. Electromechanical potentials in cortical bone. I. A continuum approach. J Biomech 20:261–270.

Schaffler MG, Burr DB, Jungers WL, Ruff CB. 1985. Structural and mechanical indicators of limb specialization in primates. Folia Primatol 45:61–75.

Shelton DR, Gibeling JC, Martin RB, Stover SM. 2000. Fatigue crack growth rates in equine cortical bone. Conference Proceedings of the American Society of Biomechanics 24th Annual Meeting, Chicago, IL. p 247–248.

Skedros JG, Bloebaum RD, Bachus KN, Boyce TM, Constantz B. 1993a. Influence of mineral content and composition on graylevels in backscattered electron images of bone. J Biomed Mater Res 27:57–64.

Skedros JG, Ota D, Bloebaum RD. 1993b. Mineral content analysis of tension/compression skeletal systems: indications of potential strain-specific differences. J Bone Miner Res 8(Suppl 1):789.

Skedros JG. 1994. Collagen fiber orientation in skeletal tension/compression systems: A potential role of variant strain stimuli in the maintenance of cortical bone organization. J Bone Miner Res 9(Suppl 1):S251.

Skedros JG, Bloebaum RD, Mason MW, Bramble DM. 1994a. Analysis of a tension/compression skeletal system: possible strain-specific differences in the hierarchical organization of bone. Anat Rec 239: 396–404.

Skedros JG, Mason MW, Bloebaum RD. 1994b. Differences in osteonal micromorphologies between tensile and compressive cortices of a bending skeletal system: indications of potential strain-specific differences in bone microstructure. Anat Rec 239:405–413.

Skedros JG, Mason MW, Nelson MC, Bloebaum RD. 1996a. Evidence of structural and material adaptation to specific strain features in cortical bone. Anat Rec 246:47–63.

Skedros JG, Dietch KC, Zirovich MD, Mason MW. 1996b. Uniform osteocyte lacuna population densities in a limb bone with non-uniform customary strain milieu and heterogeneous material organization. J Bone Miner Res 11(Suppl 1):S268.

Skedros JG, Su SC, Bloebaum RD. 1997. Biomechanical implications of mineral content and microstructural variations in cortical bone of horse, elk and sheep calcanei. Anat Rec 249:297–316.

Skedros JG, Kuo TY. 1999. Ontogenetic changes in regional collagen fiber orientation suggest a role for variant strain stimuli in cortical bone construction. J Bone Miner Res 14(Suppl 1):S441.

Skedros JG, Hughes PE, Nelson K, Winet H. 1999. Collagen fiber orientation in the proximal femur: challenging Wolff's tension/compression interpretation. J Bone Miner Res 14(Suppl 1):S441.

Skedros JG. 2000. Do BMUs adapt osteon cross-sectional shape for habitual tension vs. compression loading? J Bone Miner Res 15(Suppl 1):S347.

Skedros JG, Dayton MR, Bachus KN. 2000a. Relative effects of collagen fiber orientation, mineralization, porosity, and percent and population density of osteonal bone on equine cortical bone mechanical properties in mode-specific loading. Conference Proceedings of the American Society of Biomechanics 24th Annual Meeting, Chicago, IL. p 173–174.

Skedros JG, Hunt KJ, Gingell D. 2000b. Changes in osteocyte densities during skeletal organogenesis. J Bone Miner Res 15(Suppl 1):S459.

Skedros JG, Hunt KJ, Attaya EN, Zirovich MD. 2000c. Uniform osteocyte lacuna population densities in a limb bone with highly non-uniform strain milieu. J Bone Miner Res 15(Suppl 1):S347.

Skedros JG. 2001. Collagen fiber orientation: a characteristic of strain-mode-related regional adaptation in cortical bone. Bone 28: S110–S111.

Skedros JG, Hunt KJ, Dayton MT, Bloebaum RD, Bachus KN. 2001a. Relative contributions of material characteristics to failure properties of cortical bone in strain-mode-specific loading: implications for fragility in osteoporosis and aging. Trans Am Soc Biomech 25:215–216.

Skedros JG, Hunt KJ, Bachus KN. 2001b. Strain-mode-specific loading of cortical bone reveals an important role for collagen fiber orientation in energy absorption. Trans Orthop Res Soc 26:519.

Skedros JG, Mason MW, Bloebaum RD. 2001c. Modeling and remodeling in a developing artiodactyl calcaneus: a model for evaluating Frost's mechanostat hypothesis and its corollaries. Anat Rec 263: 167–185.

Skedros JG. 2002. Use of predominant collagen fiber orientation for interpreting cortical bone loading history: bending vs. torsion. J Bone Miner Res 17(Suppl 1):72.

Skedros JG, Hunt KJ, Sybrowsky CL. 2002a. Ontogenetic development of the ovine calcaneus: a model for examining the relative contributions of genetic, epigenetic, and extra-genetic stimuli. J Bone Miner Res 17(Suppl 1):81.

Skedros JG, Hunt KJ, Dayton MR, Bloebaum RD, Bachus, KN. 2003a. The influence of collagen fiber orientation on mechanical properties of cortical bone of an artiodactyl calcaneus: implications for broad applications in bone adaptation. Trans Orthop Res Soc 28:411.

Skedros JG, Sybrowsky CL, Dayton MR, Bloebaum RD, Bachus KN. 2003b. The role of osteocyte lacuna population density on the mechanical properties of cortical bone. Trans Orthop Res Soc 28:414.

Skedros JG, Sybrowsky CL, Parry TR, Bloebaum RD. 2003c. Regional differences in cortical bone organization and microdamage prevalence in Rocky Mountain mule deer. Anat Rec (in press).

Smalt R, Mitchell FT, Howard RL, Chambers TJ. 1997. Induction of NO and prostaglandin E_2 in osteoblasts by wall-shear stress but not mechanical strain. Am J Physiol Endrocrinol Metab 273:E751–E758.

Smit TH, Burger EH. 2000. Is BMU-coupling a strain-regulated phenomenon? A finite element analysis. J Bone Miner Res 15:301–307.

Smit TH, Burger EH, Huyghe JM. 2002. A case for strain-induced fluid flow as a regulator of BMU-coupling and osteonal alignment. J Bone Miner Res 17:2021–2029.

Smith JW. 1960. The arrangement of collagen fibres in human secondary osteons. J Bone Joint Surg 42A:588–605.

Sokal RR, Rohlf FJ. 1995. Biometry. The principles and practice of statistics. 3rd ed. New York: W.H. Freeman and Co. 887 p.

Srinivasan S, Gross TS. 2000. Canalicular fluid flow induced by bending of a long bone. Med Eng Phys 22:127–133.

Steck R, Niederer P, Knothe Tate ML. 2000. A finite difference model of load-induced fluid displacements within bone under mechanical loading. Med Eng Phys 22:117–125.

Stover SM, Pool RR, Martin RB, Morgan JP. 1992. Histological features of the dorsal cortex of the third metacarpal bone mid-diaphysis during postnatal growth in thoroughbred horses. J Anat 1813: 455–469.

Su M, Borke JL, Donahue HJ, Warshawsky NM, Russell CM, Lewis JE. 1997. Expression of connexin 43 in rat mandibular bone and peridontal ligament PDL cells during experimental tooth movement. J Dent Res 76:1357–1366.

Su S, Skedros JG, Bloebaum RD, Bachus KN. 1999. Loading conditions and cortical construction of an artiodactyl calcaneus. J Exp Biol 202:3239–3254.

Swartz SM. 1993. Biomechanics of primate limbs. In: Gebo DL, editor. Postcranial adaptation in nonhuman primates. DeKalb, IL: Northern Illinois University Press. p 5–42.

Takano Y, Turner CH, Owan I, Martin RB, Lau ST, Forwood MR, Burr DB. 1999. Elastic anisotropy and collagen orientation of osteonal bone are dependent on the mechanical strain distribution J Orthop Res 17:59–66.

Turner CH, Owan I, Alvey T, Hulman J, Hock JM. 1998. Recruitment and proliferative responses of osteoblasts after mechanical loading *in vivo* determined using sustained-release bromodeoxyuridine. Bone 22:463–469.

Turner CH, Wang T, Burr DB. 2001. Shear strength and fatigue properties of human cortical bone determined from pure shear tests. Calcif Tissue Int 69:373–378.

van der Meulen MCH, Ashford Jr MW, Kiratli BJ, Bachrach LK, Carter DR. 1996. Determinants of femoral geometry and structure during adolescent growth. J Orthop Res 14:22–29.

Vashishth D, Verborgt O, Divine G, Schaffler MB, Fyhrie DP. 2000. Decline in osteocyte lacunar density in human cortical bone is associated with accumulation of microcracks with age. Bone 26: 375–380.

Vashishth D, Gibson G, Kimura J, Schaffler MB, Fyhrie DP. 2002. Determination of bone volume by osteocyte population. Anat Rec 267:292–295.

Wainwright SA, Biggs WD, Currey JD, Gosline JM. 1982. Mechanical design in organisms. Princeton, NJ: Princeton University Press. 436 p.

Wang L, Fritton SP, Cowin SC, Weinbaum S. 1999. Fluid pressure relaxation depends upon osteonal microstructure: modeling an oscillatory bending experiment. J Biomech 32:663–672.

Weinbaum S, Cowin SC, Zeng Y. 1994. A model for the excitation of osteocytes by mechanical loading-induced bone fluid shear stresses. J Biomech 27:339–360.

Woo SLY, Keui SC, Amiel D, Gomez MA, Hayes WC, White FC, Akeson WH. 1981. The effect of prolonged physical training on the properties of long bone: a study of Wolff's law. J Bone Joint Surg 63A:780–787.

Yeni YN, Norman TL. 2000. Calculation of porosity and osteonal cement line effects on the effective fracture toughness of cortical bone in longitudinal crack growth. J Biomed Mater Res 51:504–509.

Yeni YN, Vashishth D, Fyhrie D. 2001. Estimation of bone matrix apparent stiffness variation caused by osteocyte lacunar size and density. J Biomech Eng 123:10–17.

Yeni YN, Fyhrie DP. 2002. Fatigue damage-fracture mechanics interaction in cortical bone. Bone 30:509–514.

You J, Yellowley CE, Donahue HJ, Zhang Y, Chen Q, Jacobs CR. 2000. Substrate deformation levels associated with routine physical activity are less stimulatory to bone cells relative to loading-induced oscillatory fluid flow. J Biomech Eng 122:387–393.

You L, Cowin SC, Schaffler MB, Weinbaum S. 2001. A model for strain amplification in the actin cytoskeleton of osteocytes due to fluid drag on pericellular matrix. J Biomech 34:1375–1386.